MODELING WATER REMOVAL FROM FISCHER-TROPSCH PRODUCTS USING GLYCEROL

Redeem Valoyi

A dissertation submitted to the Faculty of Engineering and the Built Environment, University of the Witwatersrand, Johannesburg, in fulfilment of the requirements for the degree of Master of Science.

Johannesburg, 2011

DECLARATION

I declare that this dissertation is my own, unaided work, unless otherwise stated. It is being submitted for the degree of Master of Science in the University of the Witwatersrand, Johannesburg. It has not been submitted before for any degree or examination in any other university.

_____

Redeem Valoyi

_____ day of _____ 2011

ABSTRACT

The focal point of this dissertation was to study the removal of water from a Fischer-Tropsch (FT) product stream using glycerol. The Fischer-Tropsch reaction forms water as one of the products, and the concentration of water keeps on increasing with increasing conversion. Therefore there is a need to remove water from the FT product stream in order to prevent a decline in catalyst activity and to keep the concentration of water within acceptable limits. Glycerol was found to be suitable for the removal of water from an FT product stream because of its property to attract moisture and to hold it.

The process to remove water from an FT product stream using glycerol was synthesized and simulated on Aspen Plus under typical operating conditions of a commercial Fischer-Tropsch process. The simulation was conducted by contacting a typical reactor product stream with liquid glycerol. Three thermodynamic property models were used for the process simulation on Aspen Plus, namely the NTRL model (Non Random two Liquid), UNIQUAC model (Universal QuAsi Chemical), and UNIFAC model (Universal Functional Activity Coefficient).These models were chosen based on their ability to predict thermodynamic data when non is available and their suitability to simulate the system under investigation.

The simulation results from Aspen Plus showed that the removal of water from the FT product stream using glycerol was a possibility; all the thermodynamic

property models predicted the same outcome. The general outcome of the simulation process was that the ability of glycerol to remove water from a Fischer-Tropsch product stream increased with pressure at a constant temperature and the amount of water it removed decreased with temperature at constant pressure.

The Aspen simulation results suggest that 91.3% of the water was removed by the glycerol at a pressure of 50 bar and a temperature of 180˚C, and 5% of the water can be removed by glycerol at 10 bar and 300˚C. The recovery of hydrocarbons by glycerol was found to be insignificant for hydrocarbons with a low carbon number (C_1–C_4). However, it was found about 40% of hydrocarbons with carbon numbers C_{10}–C_{15} were recovered into the liquid stream with glycerol because at these conditions the heavy hydrocarbons exist as a liquid rather than as a vapour phase. The process simulation also predicted that about 99% of water can be removed when the flow rate of glycerol is increased to twice the molar flow rate of water. The NTRL model was found to best fit literature data and also predicted simulation results better than the other two models.

When the simulation of the process was performed without the recycle stream of glycerol, the temperature of glycerol fed into the process had an effect on the exit temperature of the tail gas stream. When the glycerol feed temperature was low, the exit temperature of the tail gas stream was found to be lower than the FT operating temperature. However, when the process was simulated with a recycle stream of glycerol, the tail gas was found to be at a temperature that did not require the stream to be heated if it were to be recycled to the FT reactor for

further reactions to take place in order to increase conversion. Furthermore recycling glycerol did not have a significant influence in improving water recovery.

ACKNOWLEDGEMENTS

I would like to thank Professor Diane Hildebrandt and Professor David Glasser for their support and supervision.

I would also like to thank my colleagues in the COMPS Research Group for academic and social support.

I acknowledge the financial assistance from COMPS and the University of the Witwatersrand.

Above all, I would like to thank God for the strength and endurance to complete this dissertation.

TABLE OF CONTENTS

Contents **Page**

LIST OF FIGURES

LIST OF TABLES

NOMENCLATURE

Component ID	Component name	Formula
CARBO-01	Carbon-monoxide	CO
HYDRO-01	Hydrogen	H_2
WATER	Water	H_2O
GLYCE-01	Glycerol	$C_3H_8O_3$
METHA-01	Methane	CH_4
ETHAN-01	Ethane	C_2H_6
PROPA-01	Propane	C_3H_8
N-BUT-01	Butane	C_4H_{10}
N-PEN-01	Pentane	C_5H_{12}
N-HEX-01	Hexane	C_6H_{14}
N-HEP-01	Heptane	C_7H_{16}
N-OCT-01	Octane	C_8H_{18}
N-NON-01	Nonane	C_9H_{20}
N-DEC-01	Decane	$C_{10}H_{22}$
N-UND-01	Undecane	$C_{11}H_{24}$
N-DOD-01	Dodecane	$C_{12}H_{26}$
N-TRI-01	Tridecane	$C_{13}H_{28}$
N-TET-01	Tetradecane	$C_{14}H_{30}$
N-PEN-02	Pentadecane	$C_{15}H_{32}$

CHAPTER 1

INTRODUCTION

The world is desperate for energy due to economic and population growth, but the world's reserves of crude oil are depleting at an alarming rate and its price is escalating. Building Fischer-Tropsch (FT) plants that use the larger and cheaper reserves of coal and methane therefore becomes a desirable and viable alternative. However, the FT process has a number of constraints that must be considered before designing a plant. These constraints are mainly kinetics, reactor requirements, control of selectivity, and the life of catalyst. The most influential of these is the life of the catalyst in the reactor because its activity affects the selectivity and product distribution in the reactor, which in turn govern the performance of the FT process.

The decline in the FT catalyst's activity is influenced mainly by the increased concentration of water in the FT reactor (Dry, 2002). During the FT reaction, water is constantly formed as one of the products and increases over time if it is not removed from the recycle.. So there is a need to constantly remove water from the FT product stream and to keep the concentration within acceptable limits. The main focus of this research project is to model how the water concentration can be reduced in the FT reactor product stream to prevent the decline in catalyst activity and to prolong the life of the catalyst in the reactor. This will result in improved FT process performance. Current processes remove water by cooling the exit

stream from the reactor to condense out water. This is effective in terms of the water removal but the cooled stream has to be reheated to the reactor temperature before it can be recycled to the reactor to increase conversion. This leads to a process that is energy and capital intensive and to an increasingly complex operation if heat integration techniques are applied to reduce energy consumption.

In this dissertation, we will consider the removal of water, or the reduction of water concentration, by contacting the reactor product stream with a liquid that has the capacity to strip water without it reacting with the FT product stream.

CHAPTER 2

LITERATURE SURVEY

2.1 Introduction

This chapter focuses briefly on the background to the Fischer-Tropsch (FT) reaction process and the constraints associated with its operability. A review of literature on operating an FT reactor and the on methods that are currently being used to remove water from the FT product stream is presented.

2.2 Background

The production of liquid fuels from synthesis gas (syngas) was first developed by two German researchers, Franz Fischer and Hans Tropsch, while they were working at the Kaiser Wilhelm Institute in the 1920s. The process of producing liquid fuels from syngas came to be called the Fischer-Tropsch (FT) process or Fischer-Tropsch (FT) reaction. The industrial application of the FT process started in Germany and by 1938 the nine plants in operation had a combined capacity of about 660×10^3 tons per year (Dry, 2002). This production of fuel is said to have helped Germany during World War II. Dry (1999) defines FT as a process that converts a mixture of carbon monoxide (CO) and hydrogen (H_2) to a range of hydrocarbons. The mixture of CO and H_2 is generally called syngas. Dry (1999)

further notes that it has been estimated that by 2015 oil, methane and coal will account for 38%, 26% and 25% respectively of the world's energy demand.

Coal and methane can be converted to liquid fuels via the FT process by first producing syngas from these feedstocks. Methane can be reformed to syngas with steam and oxygen, either thermally or catalytically; coal can be converted to syngas in a non-catalytic gasifier, which can either be a fixed bed, fluidised bed or moving bed type. Rostrup-Nielsen (2002) notes that the production of syngas in an FT complex accounts for about 60% of the capital investment and a disproportionate share of the operating cost.

2.3 Reaction mechanism

Bartholomew (1990) describes the chemistry of FT using the following reactions.

$$CO + 3H_2 \rightarrow CH_4 + H_2O \quad (2.1)$$

$$CO + 2H_2 \rightarrow (-CH_2-) + H_2O \quad (2.2)$$

$$CO + H_2 \rightarrow CO_2 + H_2 \quad (2.3)$$

$$CO \rightarrow C + CO_2 \quad (2.4)$$

From the above reactions, it is claimed that the FT process consists of four competing reactions, but Reaction 2.2 is the most desirable one. Reaction 2.1 results in the formation of methane and Reaction 2.2 forms hydrocarbons that are

heavier than methane. Reaction 2.3 is the water-gas shift (WGS) reaction, and Reaction 2. 4 is the carbon deposition reaction.

The selectivity of these reactions depends mainly on the catalyst employed in the reaction process. There are four catalysts that can be used in an FT reaction, namely nickel (Ni), cobalt (Co), iron (Fe) and ruthenium (Ru) (Dry, 2002). Nickel catalyst, as reported in Bartholomew (1990), is more active in Reaction 2.1 than in Reaction 2.2, i.e. nickel catalyst is most selective for methane formation relative to the other three catalysts. The other three catalysts promote Reaction 2.2, which is the most desirable. However, according to the literature of Luo et al. (2009), cobalt and iron are today the only feasible commercial catalysts for an FT process.

Although Reaction 2.2 forms the main FT product, it also continuously produces water as by product. This water is reportedly known to limit conversion and prematurely deactivate the iron-based and cobalt-based catalyst through an oxidation mechanism.

2.4 The effect of water on cobalt catalysts

Rothaemel et al. (1997) studied the effect of water on cobalt-based catalysts. The study used two cobalt-based catalysts, which were an alumina supported cobalt catalyst (Co/Al_2O_3) and an alumina rhenium supported catalyst ($Co/Re/Al_2O_3$). The catalysts were treated with a water-enriched feed of carbon monoxide (CO)

and hydrogen (H_2) for 16 hours. After this period it was observed that the conversion of CO decreased by approximately 70% of the initial activity.

Botes (2009) also studied the influence of water and syngas partial pressure on the kinetics of a fresh and aged commercial alumina supported cobalt catalyst. The study was conducted by varying the water partial pressure for few hours in the FT reactor at constant hydrogen and carbon monoxide partial pressure. It was noted that the partial pressure of water in the range of 1–6 bar had no influence on the chemical reaction kinetics of syngas conversion, but did influence the product distribution. However, at higher water partial pressures, the catalyst deactivation rate was gradually increased.

2.5 The effect of water on iron-based catalysts

For iron-based catalysts it is well known that the partial pressure of water can have a negative effect on the rate of reaction (Jager and Espinoza, 1995). McDonald (1989) studied the effect of water and CO_2 on the activity and composition of iron FT catalysts. The study concludes that water build-up in the reaction results in a loss of catalyst activity and suggests that surface oxidation of the catalyst had occurred. Dry (2002) studied the effect of varying individually the partial pressures of H_2, CO, CO_2 and H_2O while total pressures varied from 0.8 to 7.6 MPa. The study concludes that increased water partial pressure had a negative effect on the FT product formation rate. The study further compares an iron-based catalyst to a cobalt-based catalyst and notes that that iron would be oxidized at

much lower partial pressures of H_2O and ratios of H_2O/H_2 than cobalt-based catalysts.

2.6 Water removal from FT processes

The water to hydrogen (H_2O/H_2) ratio increases along the length of the FT reactor and this gives cobalt catalysts a large activity advantage over iron catalysts because they are less affected by water, (Dry, 2002). Dry's study (2002) also shows that high conversions can be achieved with cobalt catalysts in a single-stage reactor without the need to recycle the tail gas or to run two stages, with water knock-out between the stages. However, it also notes that for iron-based catalysts, high conversions could also be achieved, but this requires a two-stage operation with water knock-out between the stages, together with gas recycling.

Water knock-out is done by cooling gaseous FT products and then separating the condensed liquids and non-condensable gases such as unconverted hydrogen and carbon monoxide. These gases are heated and fed to the next reactor to react to form additional hydrocarbon products. The condensed liquids generally include water and liquid hydrocarbons. This obviously increases both the capital and running costs of the iron-based catalyst FT process. However, because of the price of cobalt catalyst, it is still desirable to operate an iron-based catalyst FT process (Dry, 2002).

2.7 Developments and research on water removal from FT processes

Currently water from the FT product stream is removed by the process of cooling and heating between reactor stages. However, Fernandes (2007) mathematically modelled FT synthesis in a slurry reactor with a water permeable membrane. The results from the model showed that the water permeable membrane could be inserted in an FT reactor to remove water produced by the reaction and to prevent the WGS reaction from occurring. Most research and development in the FT area have been focused on reactor design and catalyst improvement; not much effort has been made to research specifically the removal of water from the FT product stream by means other than the methods reported above.

CHAPTER 3

PROCESS SYNTHESIS AND THE ENERGY BALANCE

3.1 Introduction

This chapter presents an analysis of the proposed process to remove water from the FT synthesis process. The thermodynamic models for vapour-liquid equilibrium (VLE) used in the process synthesis will also be discussed, particularly in relation to the integration of the process. This chapter also provides an overview of the fundamental thermodynamic concepts that will be employed in this dissertation.

3.2 Water removal medium

The ideal water removal medium for this study was a liquid with a high boiling point, which will not vaporize and which has the ability to absorb water under the operating conditions of the FT process. Different sources of technical data report that triethylene glycol (TEG), polyethylene glycol (PEG) and glycerol have water absorption ability. Bestani and Shing (1988) used the gas-liquid partition chromatography method to study the infinite-dilution activity coefficients of water in TEG, PEGs of various molecular weights, as well as glycerol and their mixtures. The results obtained from their study were used as a comparison for the relative ability of these solvents as water absorption agents at temperatures above

ambient conditions. Infinite-dilution activity coefficients of water in TEG, PEGs of molecular weights 400, 600, 1000, 1500, 7500 and glycerol were measured in the temperature range of 50˚C to about 140˚C depending on the properties of the solvent.

The conclusion of the Bestani and Shing (1988) study was that, ‘‘the molecular weight PEG (PEG 7500) had the largest water absorption capacity on a molar basis, but the lowest water absorption capacity on a mass basis, whereas the lowest molecular weight solvent, glycerol had the largest water absorption capacity on a mass basis’’. The observed trend was consistent with theoretical expectations since the dehydrating ability of a substance is primarily due to the hydroxyl (OH) groups, and glycerol has the most hydroxyl (OH) groups per unit mass compared to PEG. TEG is the most volatile solvent and significant vaporization occurs at temperatures higher than about 60˚C. However, glycerol is a hygroscopic liquid with a high boiling point, so it was selected as the water removal medium for the purpose of this work.

3.2.1 Overview of the properties of glycerol

The properties of glycerol are briefly summarized in “Physical Properties of Glycerine and its Solutions”, by the Glycerine Producers Association (1969). The term glycerine is often used to refer to the commercial product of glycerol, which possesses a small percentage of water as an impurity. Pure glycerol has a very high affinity for water and it has the ability to attract moisture from the

atmosphere and hold it. Whether glycerol is pure or a solution of a certain concentration, it will attract moisture from the atmosphere until a concentration which is in equilibrium with the atmospheric moisture is reached. Figure 1 shows a curve of relative humidity over a range of glycerol concentrations. It also shows that temperatures within the normal atmospheric limits have little effect on the equilibrium concentration when the relative humidity is kept constant.

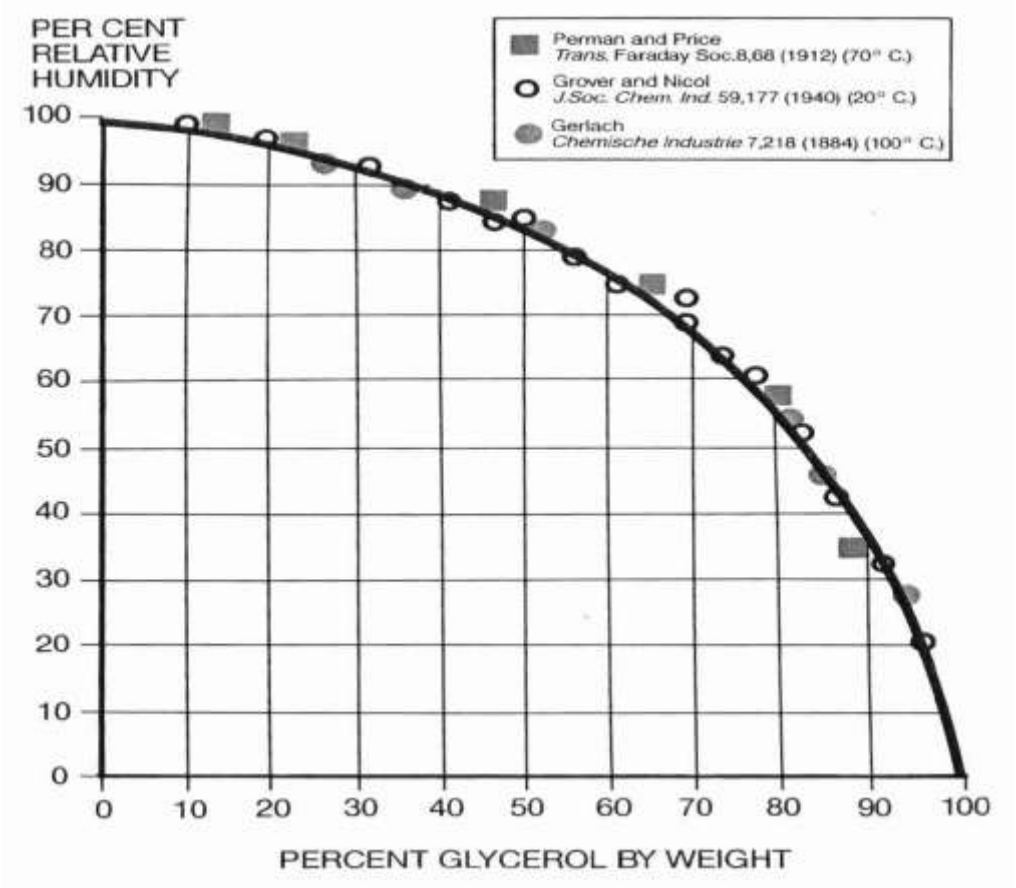

Figure 1: Relative humidity of aqueous glycerine at a temperature range of 20˚C–100˚C (adapted from Glycerine Producers Association, 1969)

Table A1 in Appendix A shows the thermal conductivity of glycerol. The trend is that the thermal conductivity increases both with water content in the glycerol as well as with an increase in temperature.

3.3 Process synthesis on the proposed water removal process

The objective of the design was to synthesize a process to decrease or remove water from the FT reactor product stream. The purpose of synthesizing such a process was to produce a stream containing the unreacted synthesis gas and hydrocarbon products without water, or at least containing very little water. This stream could then be used as feed to a subsequent reactor for further reaction to take place so as to increase the overall conversion. The current practice of water removal in the FT process is carried out by cooling the FT product stream from about 220˚C to about 25˚C; when the water has been condensed and removed from the product stream, the remaining uncondensed light gas and unconverted reactants are heated back to the operating temperature. The difference between what is being proposed and the current practice is that the tail gas stream does not need to be cooled and then reheated to the reaction temperature because we wish to remove the water from the FT product stream at the reaction temperature and pressure if possible. Figure 2 shows the overall process flow diagram for the proposed water removal from the Fischer-Tropsch product stream. The feed to the process is carbon monoxide, hydrogen gas and pure liquid glycerol. The feed to the FT reactor is assumed to be in stoichiometric proportion according to Reaction 2.2.

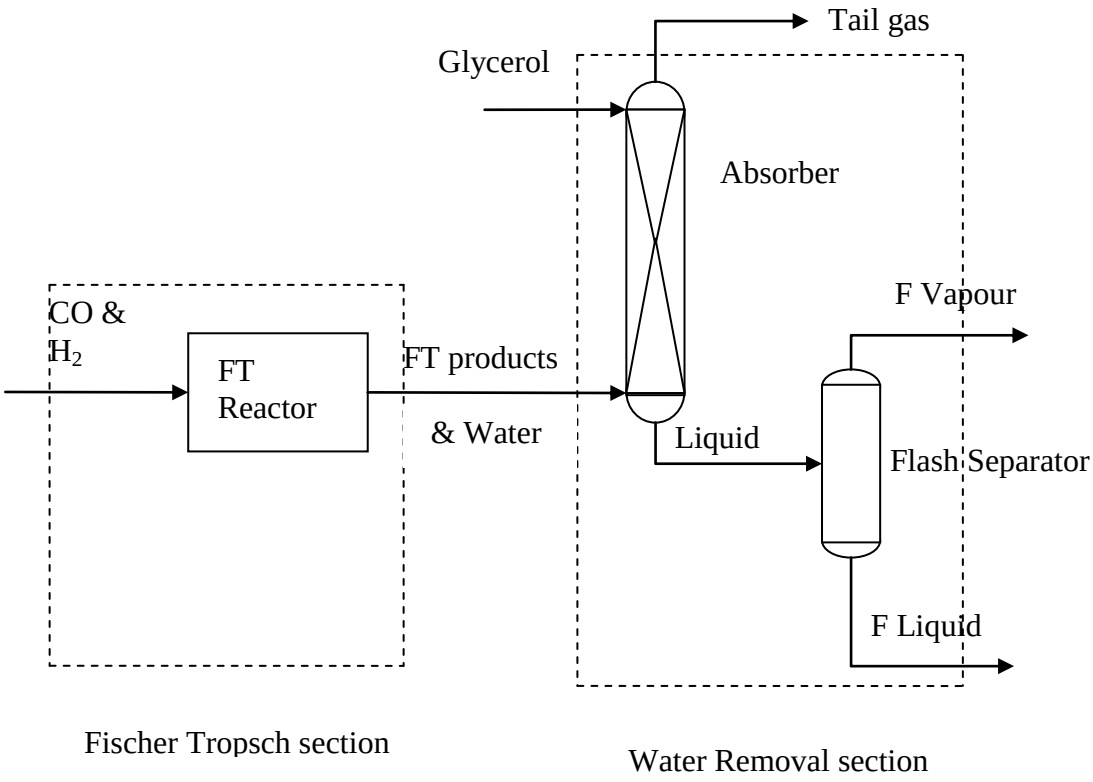

Figure 2: The proposed FT water-removal process using glycerol

The proposed process is as follows: synthesis gas is fed to an FT reactor where hydrocarbons and water are produced. The products from the FT reactor are then fed into an absorption column where glycerol is also fed into the absorber as an absorbent for the water. The purpose of liquid glycerol is to remove water selectively at the same temperature and pressure at which the FT reaction occurs. The products of the absorber are the tail gas stream and the liquid stream. The tail gas stream consists mainly of unreacted syngas and light hydrocarbons, whereas the liquid stream consists mainly of glycerol, water and any heavy hydrocarbons that are absorbed by the glycerol.

3.3.1 The energy balance over the proposed process

Figure 3 shows a schematic diagram of the water-removal process using glycerol, which is divided into two sections, namely the Fischer-Tropsch section and the water-removal section. Equation 3.1 represents the energy balance across any section of the process.

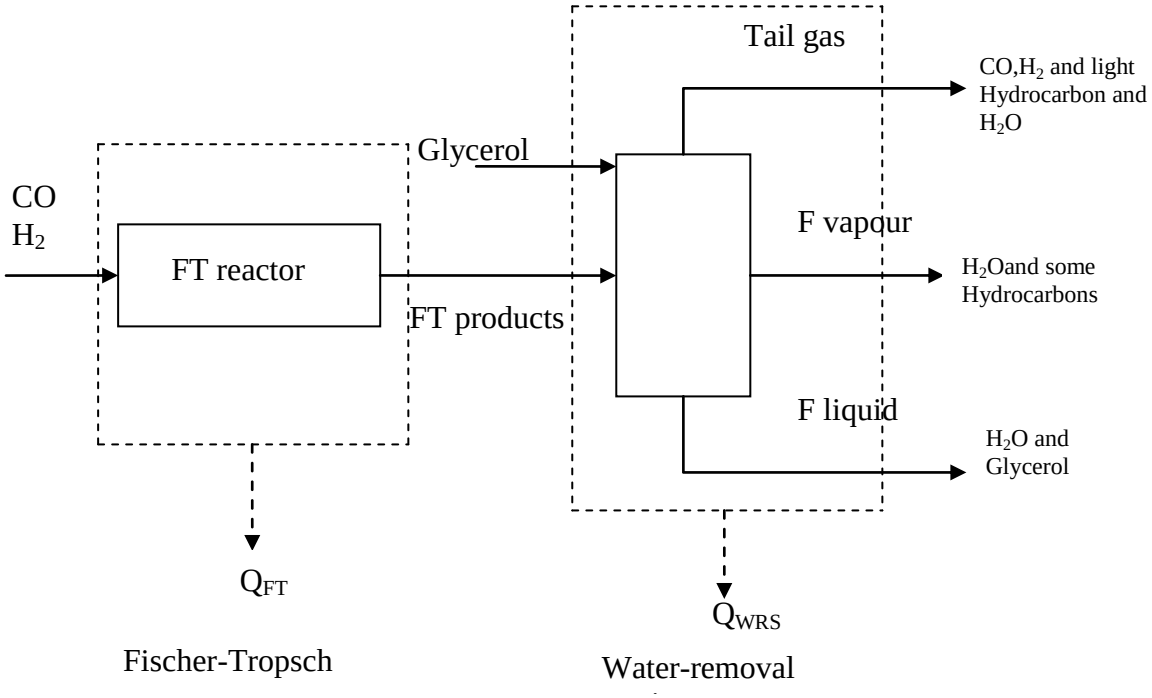

Figure 3: Schematic representation of the energy flow in the proposed process

$$\Delta H + \Delta {u^2}/{2} + g\Delta z = Q + W_S \qquad (3.1)$$

H=enthalpy

u = velocity

g = gravitational constant

z = height

Q = energy added to the system

W_S = work added to the system

Assumptions:

- $\Delta u \approx 0$
- $g\Delta z$ Negligible
- No shaft work in the system, means $W_S = 0$

The above mentioned assumptions reduce Equation 3.1 to Equation 3.2.

$$\Delta H = Q \tag{3.2}$$

In Figure 3, the energy that must be removed from the Fischer-Tropsch section is denoted by Q_{FT} and the energy for the water-removal section is denoted by Q_{WRS}. The FT reaction produces energy of about 170 kJ/mol per carbon monoxide (CO), while producing hydrocarbons and water (Krishna and Sie, 2000), which correspond to $Q_{FT,}$ the energy released by the Fischer-Tropsch section. The water-removal section requires heat to be removed from the vapour stream, leaving the flash in order to condense water and cool it to about 25˚C before it can be sent for further treatment in the water plant.

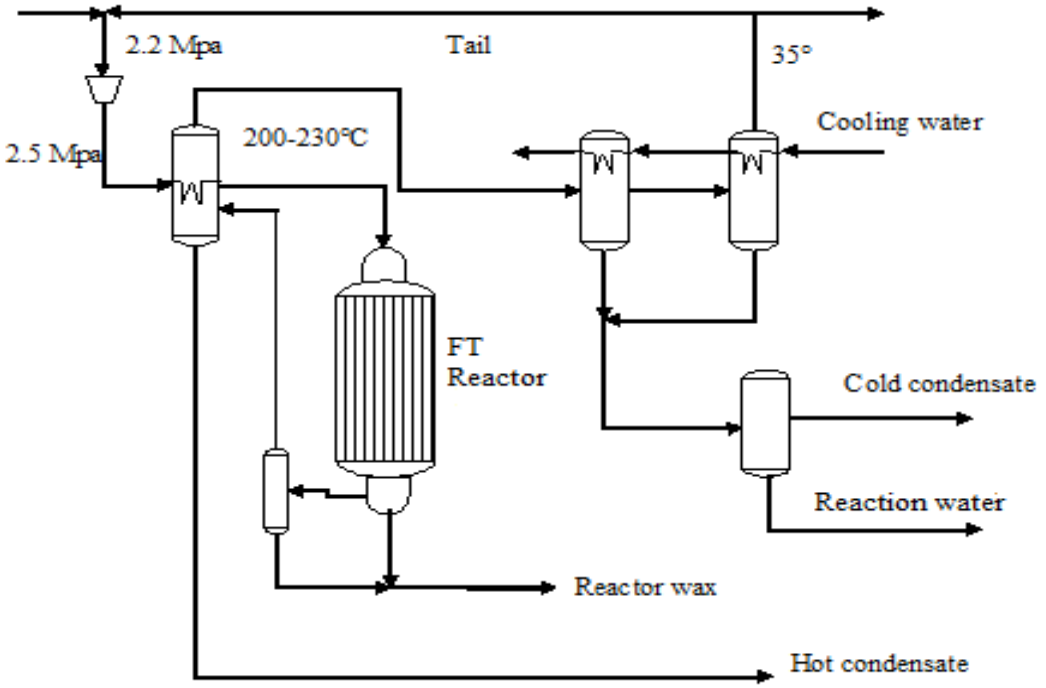

Figure 4: Section of Sasol gas loop (De Klerk, 2008)

Figure 4 shows the Sasol 1 gas loop, which is an illustration of a typical FT process in which water removal from the product stream is achieved by a series of heat exchangers. The diagram also shows that the tail gas stream has to be heated to the reactor operating temperature for recycling back into the reactor. Figure 4 is summarized by a schematic diagram, Figure 5, which simplifies the overall process and makes it easy for overall energy balance to be calculated for a typical FT process so that it can be compared to the new proposed process.

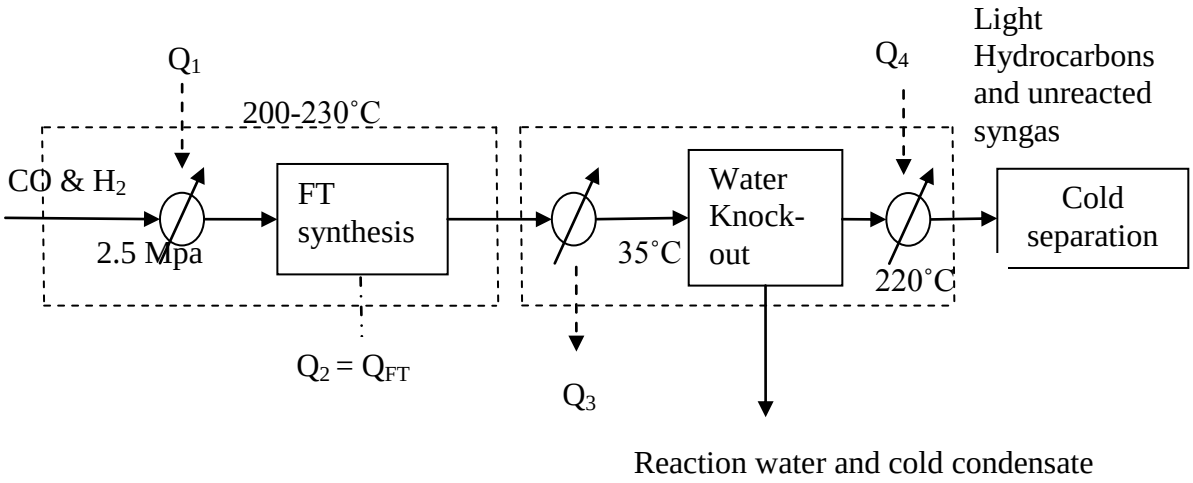

Figure 5: Overall schematic diagram of a typical Fischer-Tropsch process with water knock-out system

The energy balance Equation 3.2 also applies to the process depicted in Figure 5.Q1 represents the energy needed to heat feed Syngas to the reaction temperature and the energy that must be removed from the FT reactor is denoted by Q_{FT}; the energy that needs to be removed from the FT product stream in order to knock out water from the FT product stream is denoted by Q_3; and the energy that is needed to heat the tail gas stream to the reaction temperature is denoted by Q_4.

3.4 Concluding remarks

In this chapter we have proposed that glycerol is a suitable liquid for removing water from the FT product stream. This chapter considers the proposed process of water removal by glycerol and also shows the overall process configuration. The overall energy requirements of the process were also considered to identify the process energy flows. The typical FT process with a water knock-out system was

also considered for the purpose of comparing the energy flows in this process with the glycerol water-removal process.

The simulation of how much water the glycerol can remove from the FT process and the simulation that quantitatively compares the energy requirements of the FT process with the knock-out system and the glycerol water-removal process will be considered in the next chapter.

CHAPTER 4

PROCESS SIMULATION USING ASPEN PLUS

4.1 Introduction

This chapter shows how Aspen Plus was used to simulate the process and predict the amount of water that can be removed by glycerol. Aspen Plus is process simulation software suitable for a variety of process simulations and modelling; it also includes several databases containing physical, chemical and thermodynamic data for a wide variety of chemical compounds, as well as options to select a thermodynamic model for simulating any given chemical system.

4.2 Water-removal simulation and optimization of operating parameters for the flash

Figure 6 shows a representation of the Aspen Plus simulation flow diagram, which was used to evaluate the ability of, or the extent to which glycerol can remove water from an FT product stream.

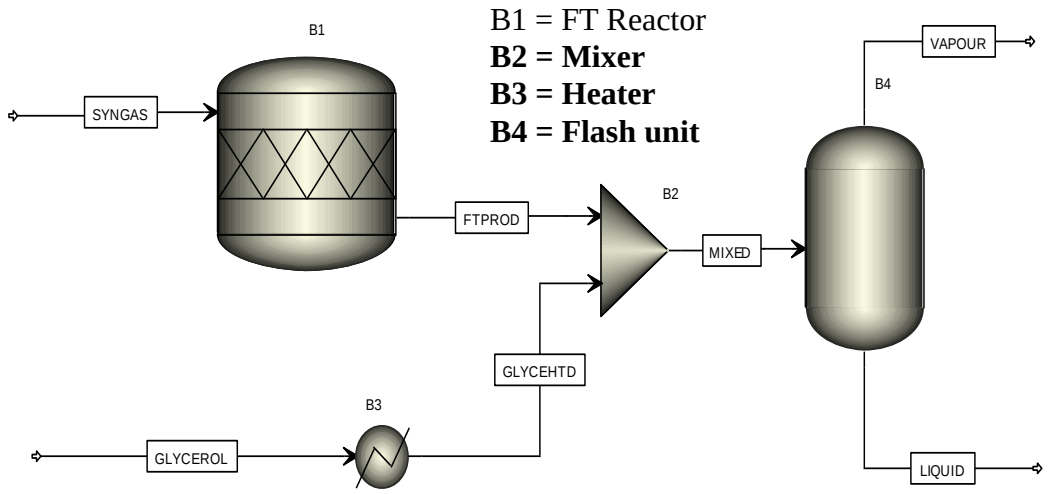

Figure 6: ASPEN simulation model to investigate the ability of glycerol to remove water under different operating conditions

Figure 6 shows that the FT product stream is mixed with glycerol and then fed into a flash unit to allow separation between the liquid and vapour phase. The liquid and vapour phase from the flash unit are assumed to be in thermodynamic equilibrium with each other for all components present in these phases.

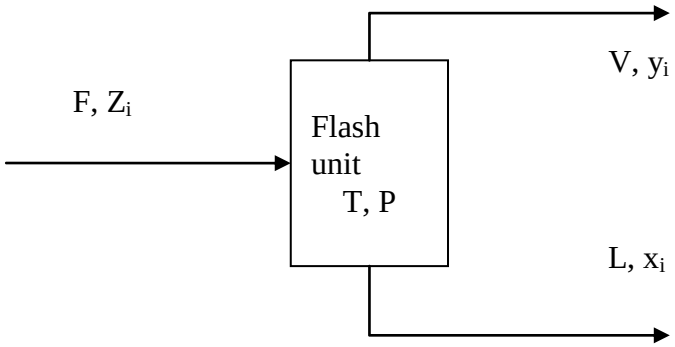

Figure 7: Representation of equilibrium flash separation

Figure 7 shows a basic representation of a flash operation unit used to set up material and energy balance around the flash unit. The overall and component

mass balance around the flash unit is described by Equations 4.1 and 4.2 respectively. The variable F denotes the molar feed flow rate into the flash, whereas L and V represent the liquid and vapour molar flow rate produced from the flash unit.

$$F = L + V \tag{4.1}$$

$$Fz_i = Lx_i + Vy_i \tag{4.2}$$

The variable z_i is the molar fraction of a particular component i in the feed stream of the flash unit; x_i and y_i represent the molar fraction of a particular component i in the liquid and vapour stream respectively. The recovery of any component to the liquid stream can be calculated from Equation 4.3.

$$Recovery\ of\ component\ i = {}^{Lx_i}/_{Fz_i} \tag{4.3}$$

However, for mass or material balance to exist, the composition of all the species present in all respective phases must sum to unity, as shown by Equations 4.4 and 4.5.

$$\sum_{i=0}^{n} x_i = 1 \tag{4.4}$$

$$\sum_{i=0}^{n} y_i = 1 \tag{4.5}$$

The vapour-liquid equilibrium ratio (K-value), as shown in Equation 4.6, is defined for a component i as the ratio of mole fraction in the vapour to mole fraction in the liquid phase (Rousseau and Ronald, 1987).

$$K_i = \frac{y_i}{x_i} \tag{4.6}$$

The extent of water removal was determined from the simulation results by calculating the water recovery according to Equation 4.3. The equilibrium distribution K-values were calculated according to Equation 4.6 in order to evaluate whether water was likely to be in the vapour or liquid phase. The theoretical K-value was calculated by assuming the liquid phase obeys Raoult's law and the gas or vapour phase obey the ideal gas law.

$$K_{i,Theory} = \frac{P_i}{P} \tag{4.7}$$

Where P_i is the partial pressure of any pure component and P is the total pressure of the system. The partial pressures of the pure components were obtained from the thermodynamic database of Aspen.

4.3 Process simulation

4.3.1 Configuration for the process using an absorber and glycerol recycle

Figure 8 is a representation of an Aspen Plus simulation flow diagram for determining the flow rate of glycerol required to remove most of the water from the product stream and also to determine the exit temperatures from the process. Contrary to figure 6, an absorber is used in figure 8 for contacting the liquid glycerol with FT products because of practical consideration of the absorption of vapour (H2O) by liquid glycerol.

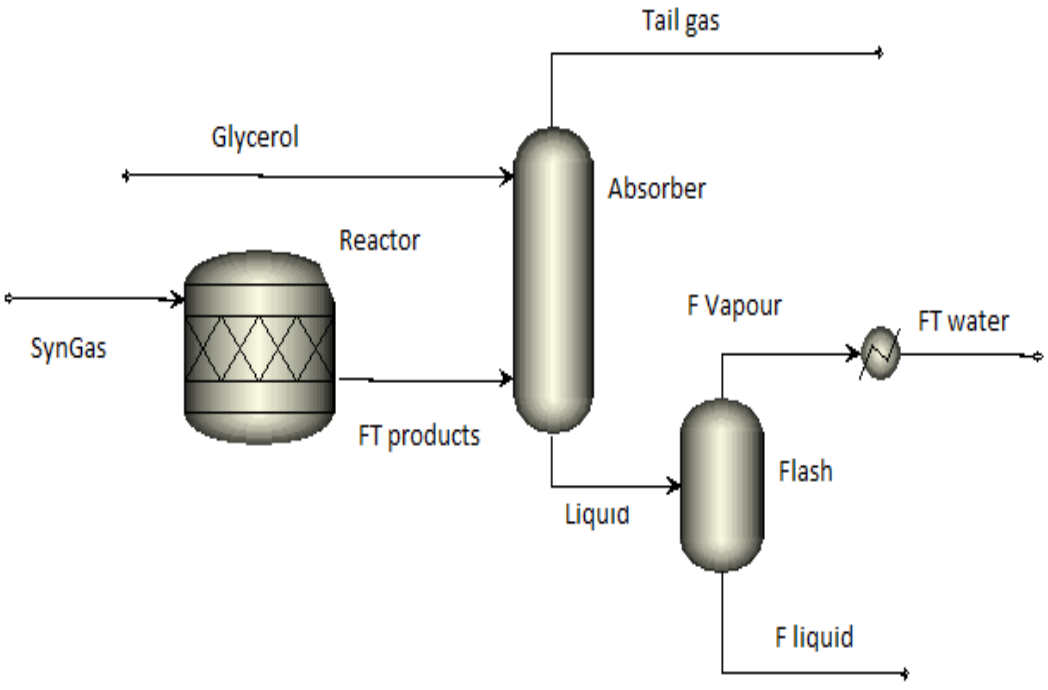

Figure 8: Aspen simulation for proposed process to remove water by glycerol

The liquid stream from the flash is predominantly composed of glycerol, and recycling it would decrease the amount of glycerol required in the fresh feed. Figure 9 shows the model used to simulate the process with the flash liquid stream being recycled.

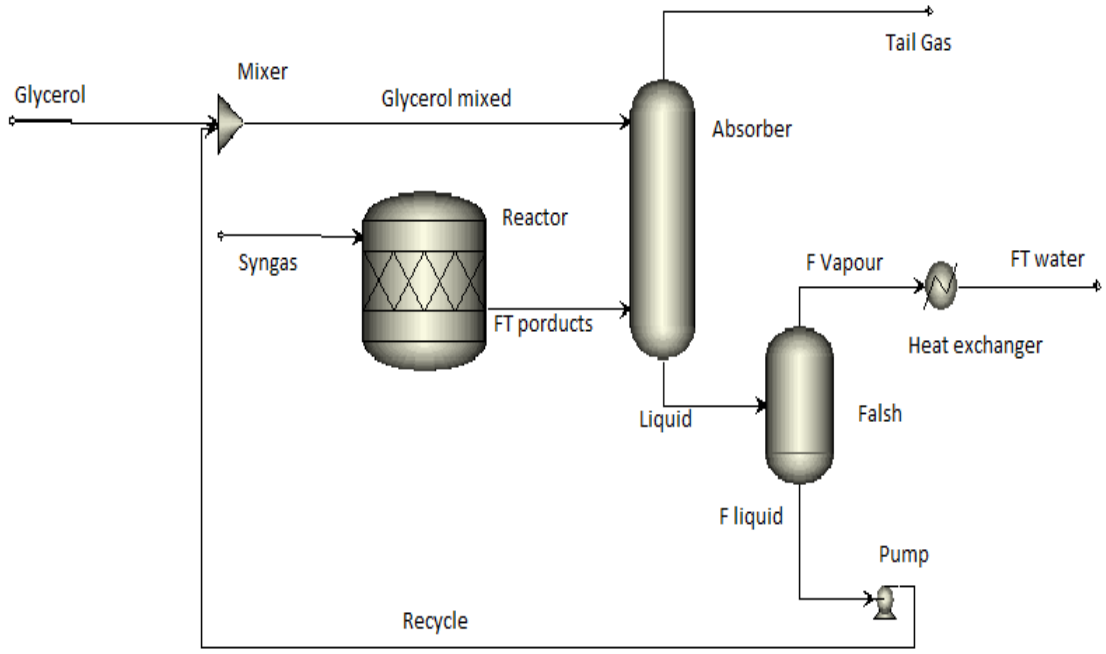

Figure 9: Aspen simulation for proposed process to remove water by glycerol with glycerol recycle stream

4.3.2 Choice of thermodynamic property model

The choice of a reliable property method for simulating processes is essential to achieving accurate results. These models are useful for predicting liquid phase non-ideality, but they require some experimental data (Rousseau and Ronald, 1987). There are various activity coefficient models that correlate the activity coefficient with its mole fraction in the liquid concerned: the NTRL model (Non

Random Two Liquid), UNIQUAC model (Universal QuAsi Chemical), and UNIFAC model (Universal Functional Activity Coefficient). ASPEN Plus has a property method assistant, which provides a more detailed way of selecting a property method, including consideration of process type. Refer to Figure A1 in Appendix A for the property method assistant. Refer to Appendix B for the simulation results.

4.3.3 The FT reactor model

The FT reactor was modelled by the stoichiometric reactor model which is a balance-based reactor and requires both atom and mass balance equations. This type of a reactor is used in situations where equilibrium data and kinetics of the reaction are unimportant. However, the heat of reaction can be calculated at reference temperature and pressure. The reaction was modelled for the production of alkanes C_1 to C_{15} by Reaction 2.2 and, for the purpose of simplicity; it was assumed that the hydrocarbon products (i.e. FT product) behave like paraffins because these are the main products in practice. The conversion of each alkane's reaction was calculated according to the Anderson Schulz-Flory distribution with an $\alpha = 0.8$; the overall conversion of carbon monoxide (CO) was assumed to be at 80%. The Anderson Schulz-Flory distribution of 0.8 and 80% overall conversion of carbon monoxide (CO) are averages of what is normally obtained in most FT experiments. The reactor temperature and pressure were varied within typical or operating ranges, that is 180˚C to 300˚C and 10 to 50 bars respectively, while keeping either one of the variables constant.

4.3.4 The absorber

Radfrac is a rigorous two or three-phase vapour liquid equilibrium column used by Aspen Plus to model absorbers for the purpose of rigorous rating and designing single columns while other columns are used for designing systems with multicolumns. The Radfrac absorber with two stages was used to model the absorption of water from the gaseous FT stream by using liquid glycerol. The numbers of stages were dependent on the flow rate of glycerol, but using more stages did not improve recovery. The absorption was modelled at the reactor operating temperature and pressure.

4.3.5 Flash separator

The flash separation unit was modelled to flash or separate water that was absorbed by the glycerol from the glycerol. The liquid product stream from the absorber was flashed at the exit temperature from the absorber by dropping the pressure from 25 bar to 1 bar. The product from the flash unit is the flash vapour stream, which is cooled to room temperature, and the flash liquid stream, which is glycerol rich.

4.4 Concluding remarks

This chapter considers the proposed process of water removal by glycerol and also illustrates the overall process configuration for the purpose of simulation using Aspen Plus. The process units that are employed in simulation were briefly discussed. The process simulation was performed using three thermodynamic property models, which were considered suitable for simulating such a process. The simulation of how much water the glycerol can remove from the FT process and the simulation that quantitatively compares the amount of glycerol required to remove a certain quantity of water were also considered. The results of the simulation process are presented and discussed in the next chapter.

CHAPTER 5

RESULTS AND DISCUSSION

5.1 Introduction

This chapter presents the simulation results of the water-removal process from the FT product stream. The Aspen Plus simulation was performed, initially without considering the recycling of glycerol. Once conditions had been optimized, the recycle was included and the process was reanalysed and optimized. The results from the Aspen Plus simulation were used to evaluate the ability of or the extent to which the glycerol can remove water from the FT product stream, which was calculated according to Equation 4.7.

5.2 Simulation results for water removal on a simple flash

The NTRL, UNIQUAC and UNIFAC thermodynamic property models were used for the Aspen simulation and the results were used to calculate water recovery to the flash liquid stream. These results are presented in Figures 10, 11 and 12 respectively. All models show that the recovery of water at a constant temperature increases with pressure, and the recovery of water at constant pressure decreases with temperature. Figure 10 shows the predicted recovery of water when using the NTRL model over a pressure range of 10 bar to 50 bar and a temperature range of

180˚C to 300˚C. The lowest predicted recovery of 0.0504 occurs at the lowest pressure of 10 bar and a temperature of 300˚C; the maximum recovery of 0.913 occurs at a pressure of 50 bar and a temperature of 180˚C. These maximum and minimum values are the attainable recoveries under these conditions and for the selected property model.

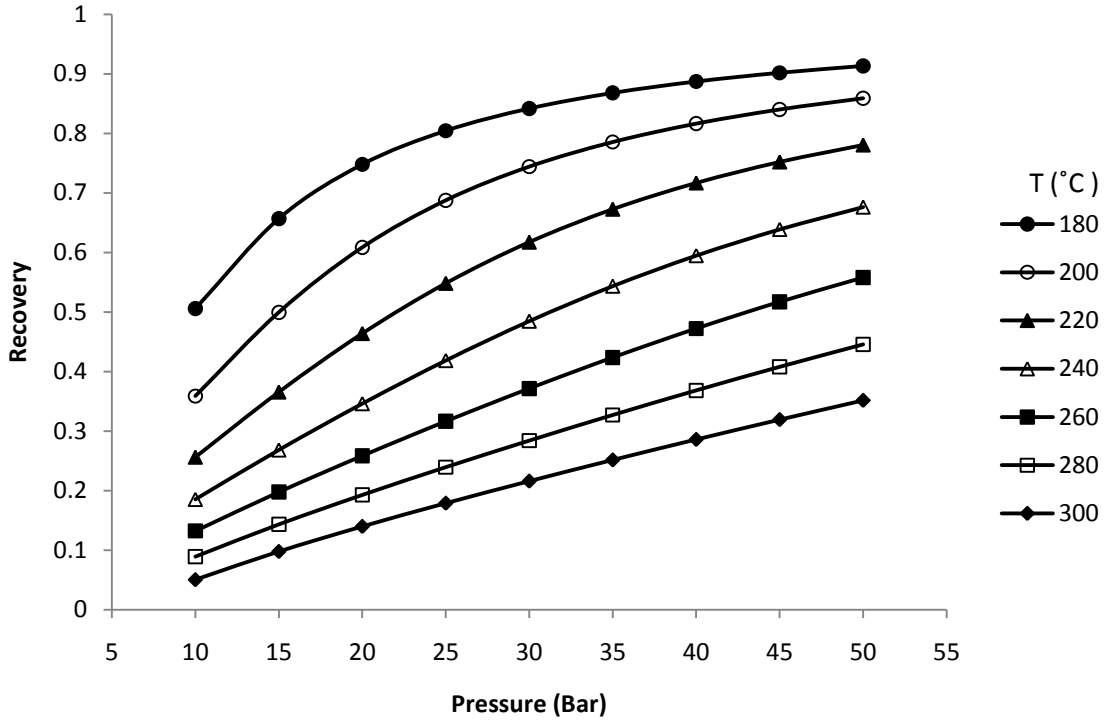

Figure 10: Effect of pressure and temperature on water recovery in a simple flash using the NTRL model.

Figure 11 shows the predicted recovery using the UNIQUAC model. This model predicts that a minimum recovery of 0.0490 is at a pressure of 10 bar and temperature of 300˚C; the highest recovery is 0.908 at 50 bar and 180˚C. The overall minimum and maximum recoveries of water from Aspen simulation using the UNIQUAC thermodynamic property model are slightly lower compared to the

recoveries of the NTRL model by 2.77% and 0.547% respectively, but these models agree very closely.

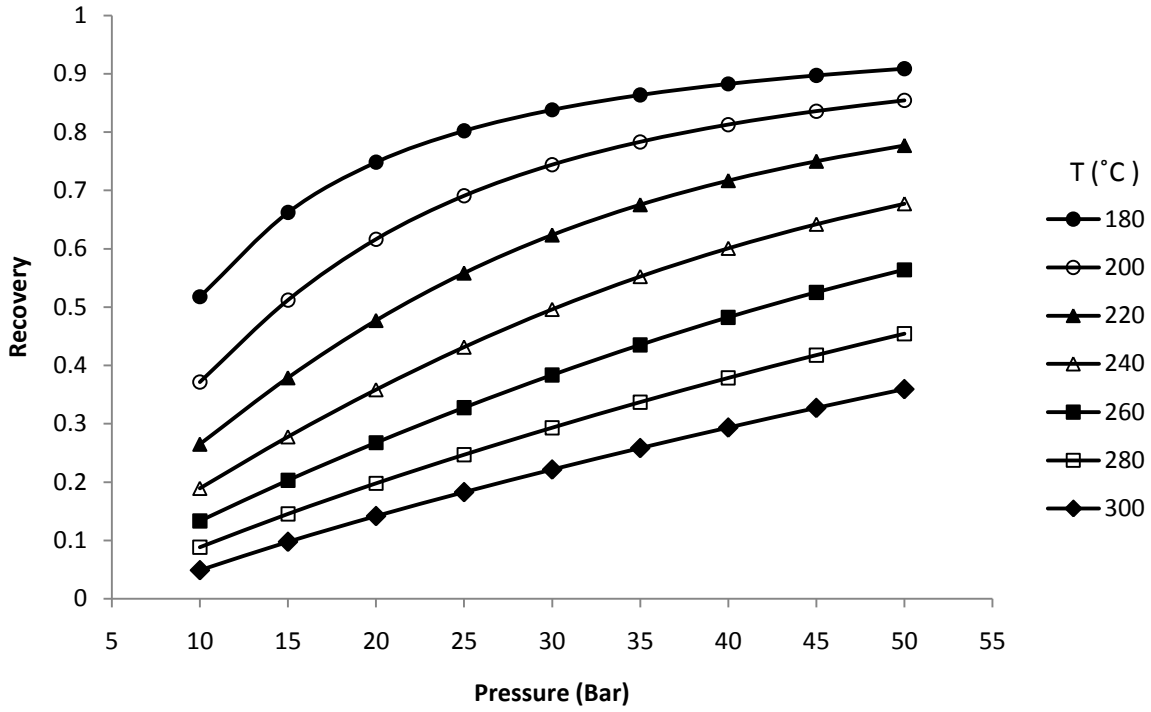

Figure 11: Effect of pressure and temperature on water recovery in a simple flash using the UNIQUAC model

Figure 12 shows the predicted recovery using the UNIFAC model: a minimum recovery of 0.0154 is at 10 bar and 300˚C, and the maximum recovery of 0.861 occurs at 50 bar and 180˚C. Comparing Figure 12 to Figures 10 and 11, the overall minimum and maximum recovery of water has decreased roughly by 68% and 5.6% respectively. Even though the overall minimum and maximum recovery of water has decreased significantly, there is a qualitative commonality between Figures 10, 11 and 12 that indicates similar trends of water recovery at various

temperatures and pressure. There is, however, a significant difference between these graphs in the quantitative values for the recovery of water.

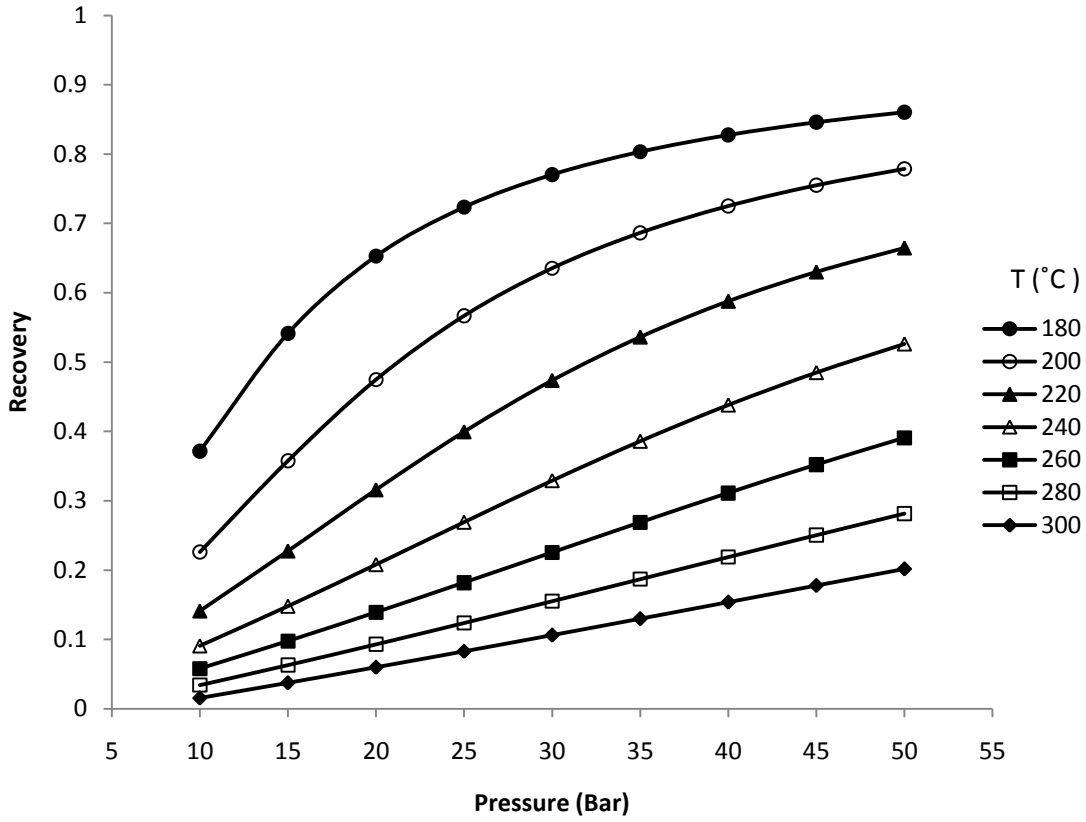

Figure 12: Effect of pressure and temperature on water recovery in a simple flash using the UNIFAC model

The difference between the results obtained from the NTRL, UNIQUAC and UNIFAC thermodynamic property models may be attributed to the fact that the NTRL and UNIQUAC property models assume the ideal gas law in the vapour phase and Henry's law in the liquid phase, whereas the UNIFAC property model applies a Redlich Kwong equation of state to the vapour phase and Henry's law to the liquid phase. All three property models predict that water recovery at constant

temperature increases with pressure and decreases with temperature at constant pressure.

5.2.1 Predicted equilibrium distribution coefficient for water in glycerol

Figure 13 shows the predicted equilibrium constant, (K-value), of water obtained from the NTRL thermodynamic model.

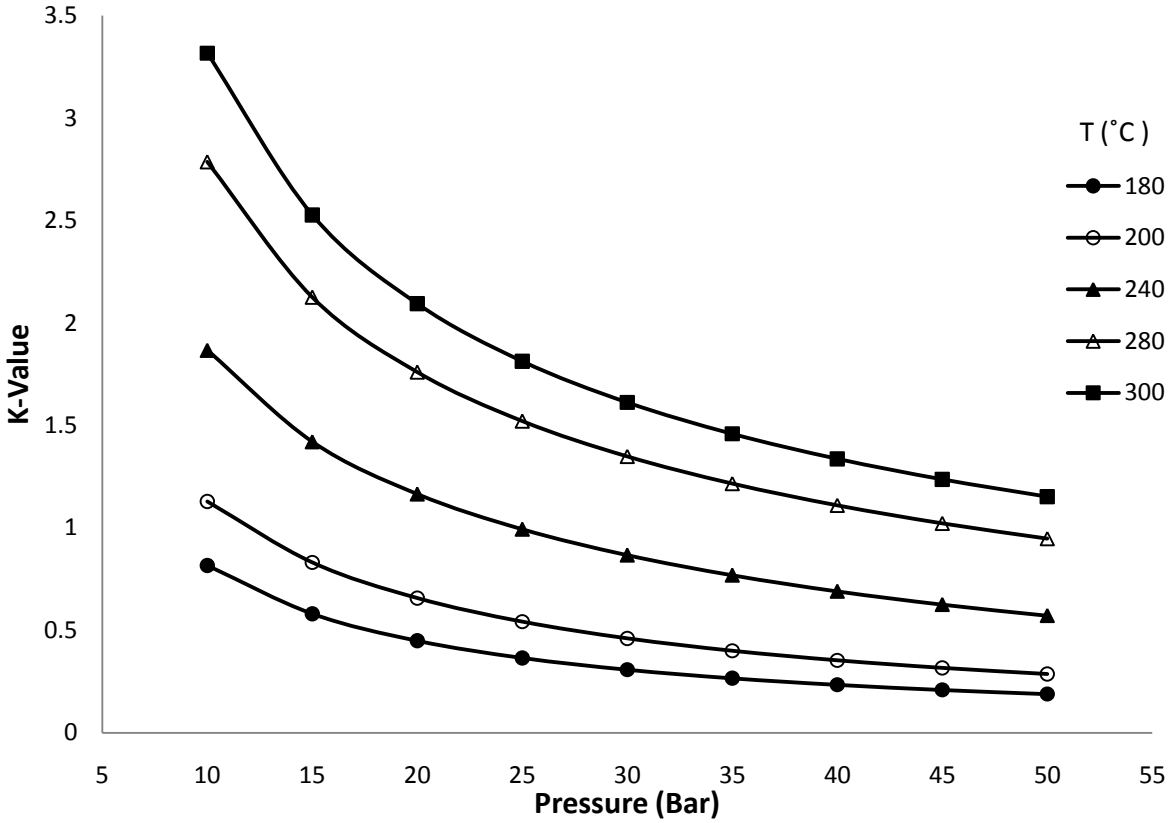

Figure 13: Predicted K-value for water at various temperatures and pressures, using the NTRL model in a simple flash

Figure 13 shows that the K-value increases with increasing temperature, which implies that there would be less water in the vapour phase at low temperature and higher pressure. The general trends in Figure 13 suggest that at higher temperature

and low pressure, there would be more water in the vapour phase and less water in the liquid phase.

Figure 14 shows the equilibrium K-values for water obtained from Aspen Plus simulations using various thermodynamic models at 180˚C. The K-values obtained from the UNIQUAC and UNIFAC models are the same, as their plots lie on top of each other. However, these K-values are slightly lower than those obtained from the NTRL property model at low pressure; as pressure increases, these values converges at a pressure of about 40 bar.

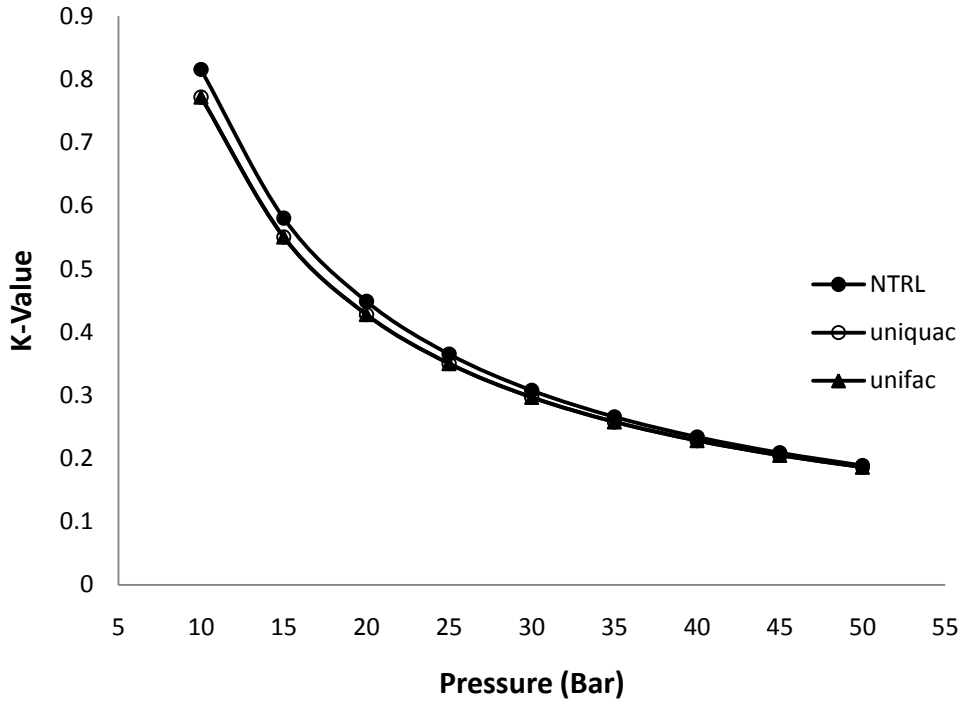

Figure 14: Predicted K-values for water in glycerol at 180˚C for the different property models

The K-values of water for various temperatures and property models are presented in Table B1.1 to Table B1.3 in Appendix B1.The trend of equilibrium K-values for the UNIQUAC and UNIFAC models are similar to that of the NTRL

thermodynamic model. All models predict that when the temperature is increased at a specific pressure, the K-value increases, which means that there will be less water in the liquid phase compared to the vapour phase. The models also predict that as the pressure increases at constant temperature, & K-value decreases. The implication of the decreasing K-value is that there would be more water in the liquid phase relative to the vapour phase.

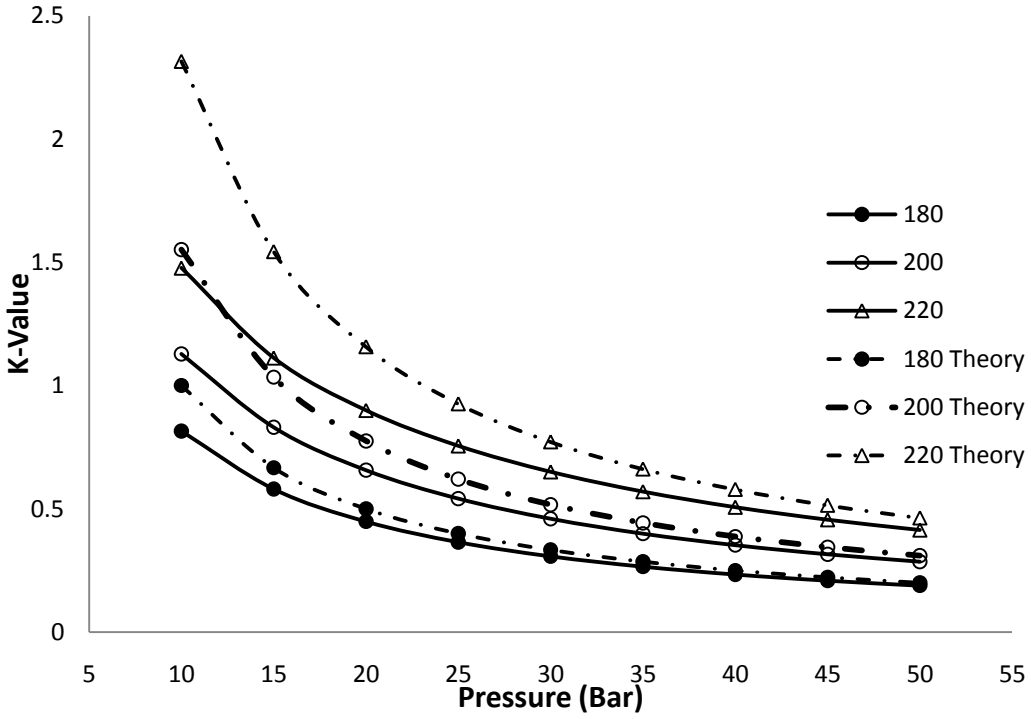

Figure 15: Comparison of predicted K-values for water in glycerol using the NTRL model and K-values predicted using Raoult's law.

Figure 15 shows the comparison of K-values calculated from the NTRL model and those predicted using Raoult's law. The observation from the plots is that the K-values calculated using Raoult's law at low pressure are higher than those calculated from the simulation results using the component mole fractions in the gas & liquid phases, but as pressure increases the Raoult's law K-values tend to approach the K-values calculated from the simulation results. At a pressure of 10

bar and temperatures of 180˚C, 200˚C and 220˚C, the Raoult's law K-values are higher than the simulated K-values by 23.2%, 37.5% and 56.7% respectively. It is evident that the difference between the theoretical and the simulated K-values increases with temperature and decreases with increasing pressure. Therefore this suggests that the assumption of ideal behaviour is not correct.

5.2.2 Comparison of simulation results with literature data

Soujanya et al., 2009 measured the vapour liquid equilibrium data of water and glycerol at sub atmospheric pressure ranging from 14.19 Kpa to 95.3 Kpa and the data was compared to the simulation results of NTRL, UNIQUAC and UNIFAC. The Literature data plotted on the Figure 16 & 17 shows more water mole fraction at low pressure and temperature and that water mole fraction in the liquid phase decreases with increasing temperature at fixed pressure.

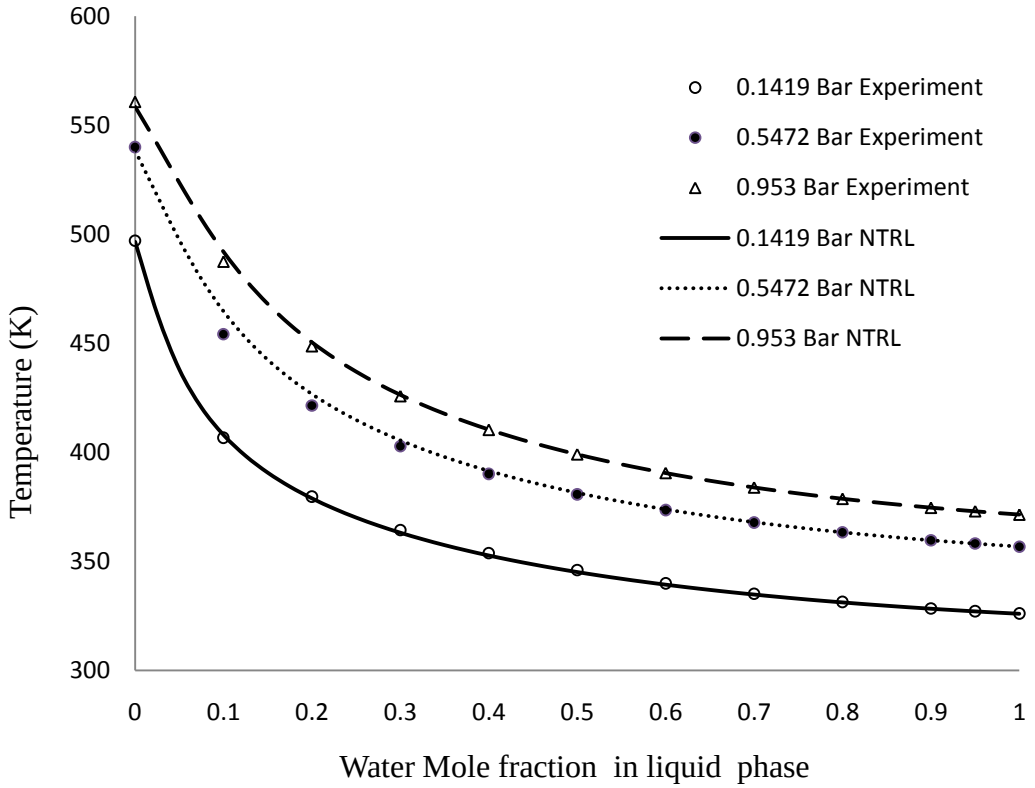

Figure 16: Comparison of Literature data with NTRL simulation results

Comparing NTRL & UNIQUAC simulation results with literature data on Figure 16 & 17, it can be observed that both Thermodynamic property models represents the literature data adequately, with two points at a pressure of 0.5472 bar not fitting with the model. Qualitatively NTRL represents the data much better compared to UNIQUAC because it deviates from literature data by 3.4% while UNIQUAC deviates by about 5.8%.

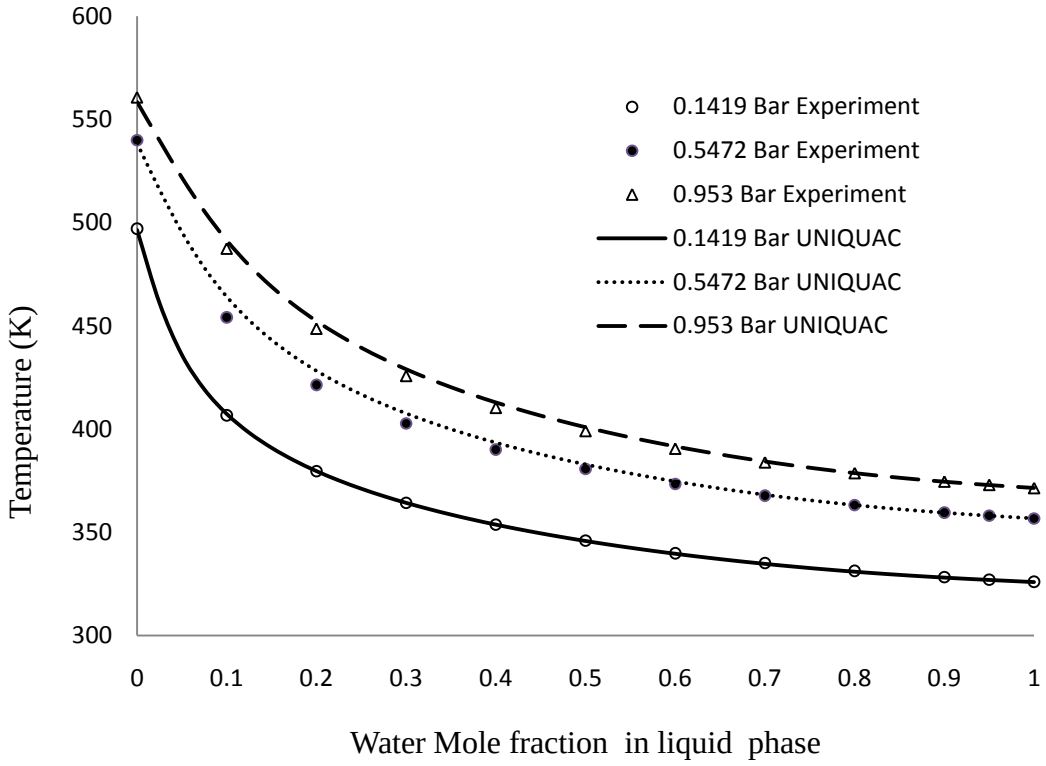

Figure 17: Comparison of Literature data with UNIQUAC simulation results

The UNIFAC model results on Figure 18 shows that at a fixed pressure and low temperature the model fits literature data, however there are significant deviations between the model results and literature data at higher temperatures. The increase in pressure shows no clear effect on the fit, but the implication of poor fit by UNIFAC is that it is not reliable at high temperature. The NTRL and UNIQUAC model are predicting the results better than UNIFAC, but NTRL provides a better fit than UNIQUAC.

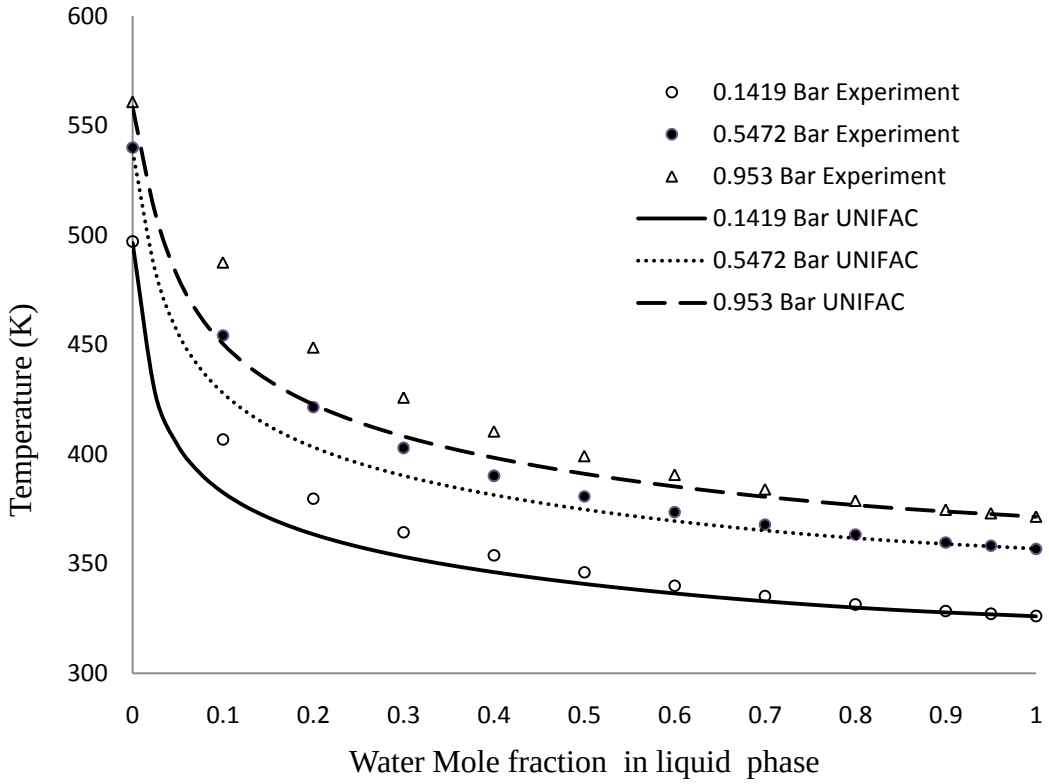

Figure 18: Comparison of Literature data with UNIFAC simulation results

5.3 Simulation results for absorption of hydrocarbons in glycerol in a simple flash

Ideally the glycerol should selectively absorb water and not the hydrocarbons in the exit stream from the reactor. In this section we use various thermodynamic models to predict the ability of glycerol to absorb the hydrocarbon products.

5.3.1 Hydrocarbon recovery

Figure 19 shows the NTRL thermodynamic property model results for the recovery of hydrocarbons (C_1–C_{15}) into the liquid stream of the flash unit. It is

observed that the recovery of the hydrocarbons at a specific temperature increases with increasing carbon number and increasing pressure. The lighter hydrocarbon methane has a maximum recovery of 0.0658 at 50 bar and 180˚C, whereas the heavier hydrocarbons are completely recovered into the liquid stream. The general trend for predicted recovery in Figure 19 is that the recovery of hydrocarbons increases with an increase in pressure at a specific temperature. Figures B2.1 to B2.4 in Appendix B2 show that the general trend of recovery at a specific pressure decreases with an increase in temperature.

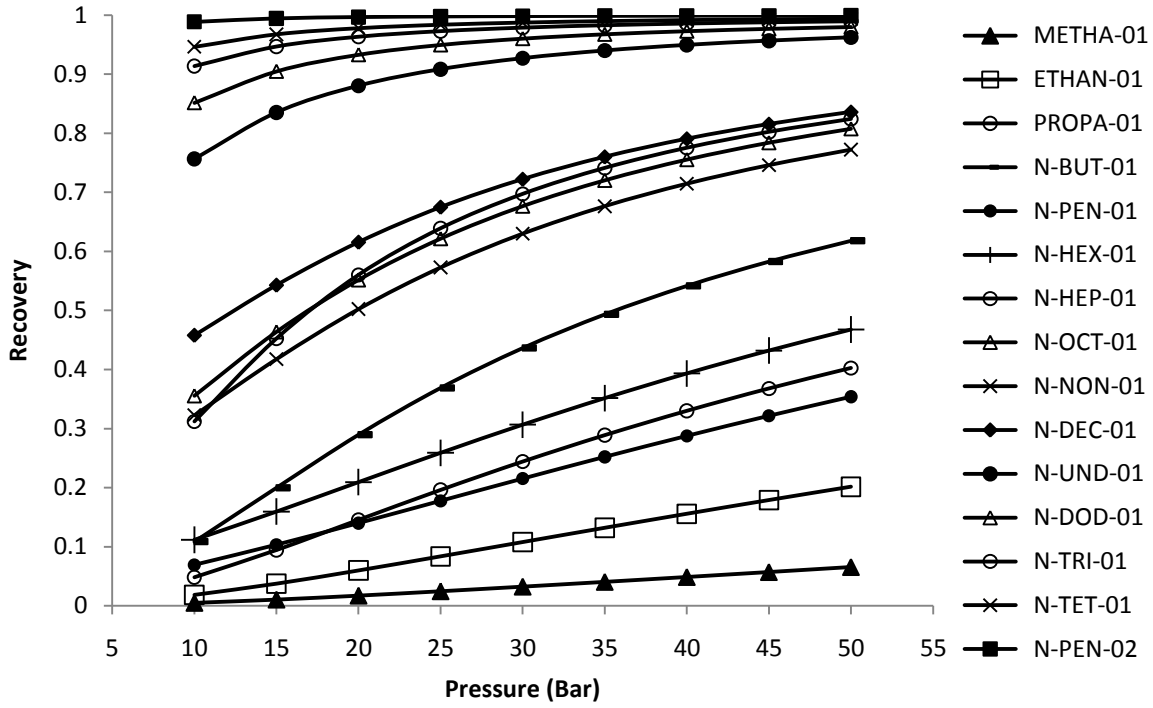

Figure 19: Predicted recovery of hydrocarbons to the liquid stream in a flash unit using the NTRL model at 180˚C

Figure 20 shows the predicted recovery of hydrocarbons (C_1–C_{15}) into the liquid stream of the flash unit at 300˚C when using the NTRL thermodynamic property

model. Figure 20 shows that recovery of hydrocarbons decrease substantially at the higher flash temperature. The difference between Figures 19 and 20 may be attributed to fact that, at 300˚C, the heavier hydrocarbons are likely to be in vapour phase, but as pressure is increased, a higher recovery is obtained.

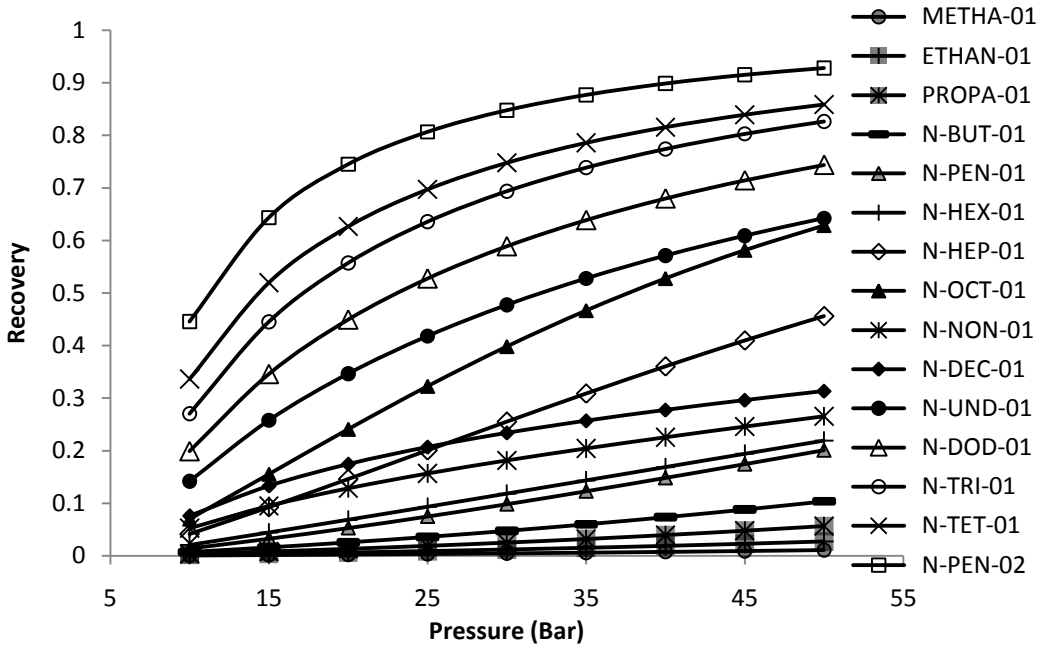

Figure 20: Predicted recovery of hydrocarbons to the liquid stream in a flash unit using the NTRL model at 300˚C

Figure 21 shows, when using the UNIQUAC thermodynamic property model, the predicted recovery of hydrocarbons (C_1–C_{15}) into the liquid stream of the flash unit at 300˚C. Figure 21 shows that the recovery of some hydrocarbons decreases slightly with an increase in pressure and thereafter increases with an increase in pressure at a fixed temperature. The recovery of methane is at a maximum of 0.0655 at 50 bar and 300˚C, and the heavier hydrocarbons are completely recovered into the liquid stream. The general recovery trend shown in Figure 21 is the same as that of Figure 20. Figures B2.5 to B2.8 in Appendix B2 show that the

general recovery trend at a specific pressure decreases with an increase in temperature.

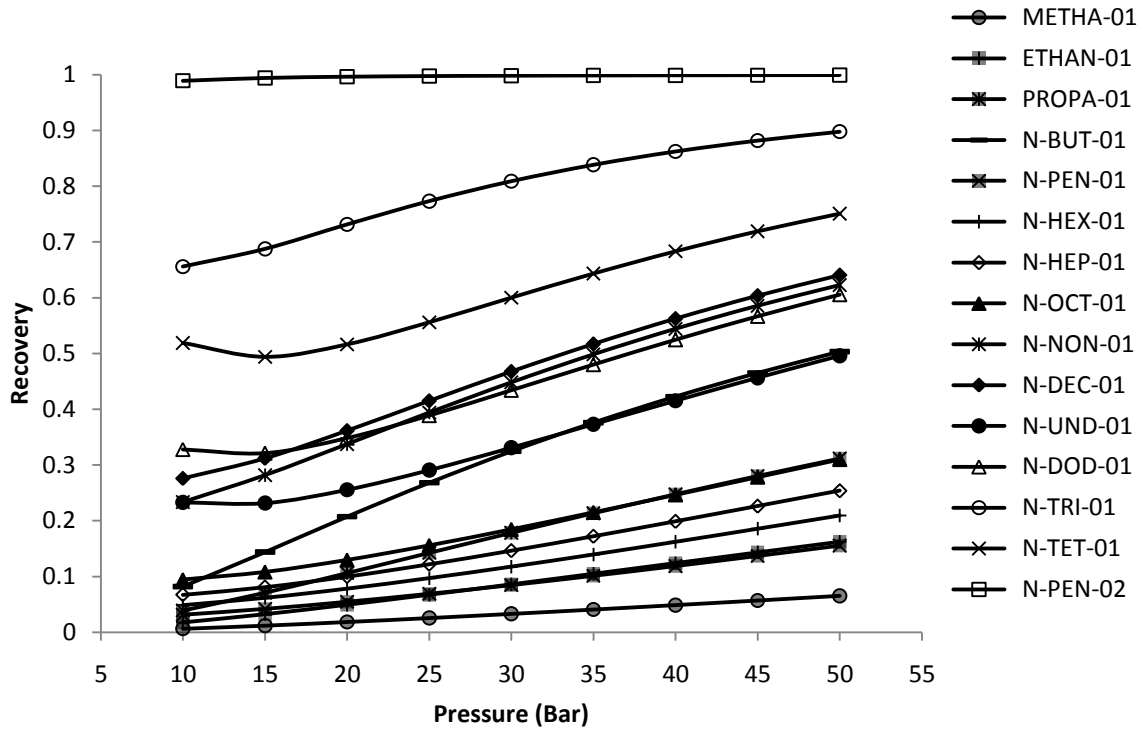

Figure 21: Predicted recovery of hydrocarbons to the liquid stream in a flash unit using the UNIQUAC model at 300˚C.

Figure 22 shows the predicted recovery of hydrocarbons (C_1–C_{15}) into the liquid stream of the flash unit when using the UNIFAC thermodynamic property model . It is observed that the recovery of the (C_2–C_{15}) hydrocarbons at a specific temperature and pressure decreases with an increase in carbon number. However, methane does not follow the observed general trend and has a maximum recovery of 0.0371 at 50 bar and 180˚C. The heavier hydrocarbon has a maximum recovery of 0.0270 at 50 bar and 180˚C. UNIFAC is predicting conflicting results to NTRL & UNIQUAC because the process conditions exceeded the limitation of the

UNIFAC model. The UNIFAC model is suitable for simulating the system in the process, but the conditions of the model are such that the pressure should not be above 10 bar and temperature should be less than 150 ˚C.

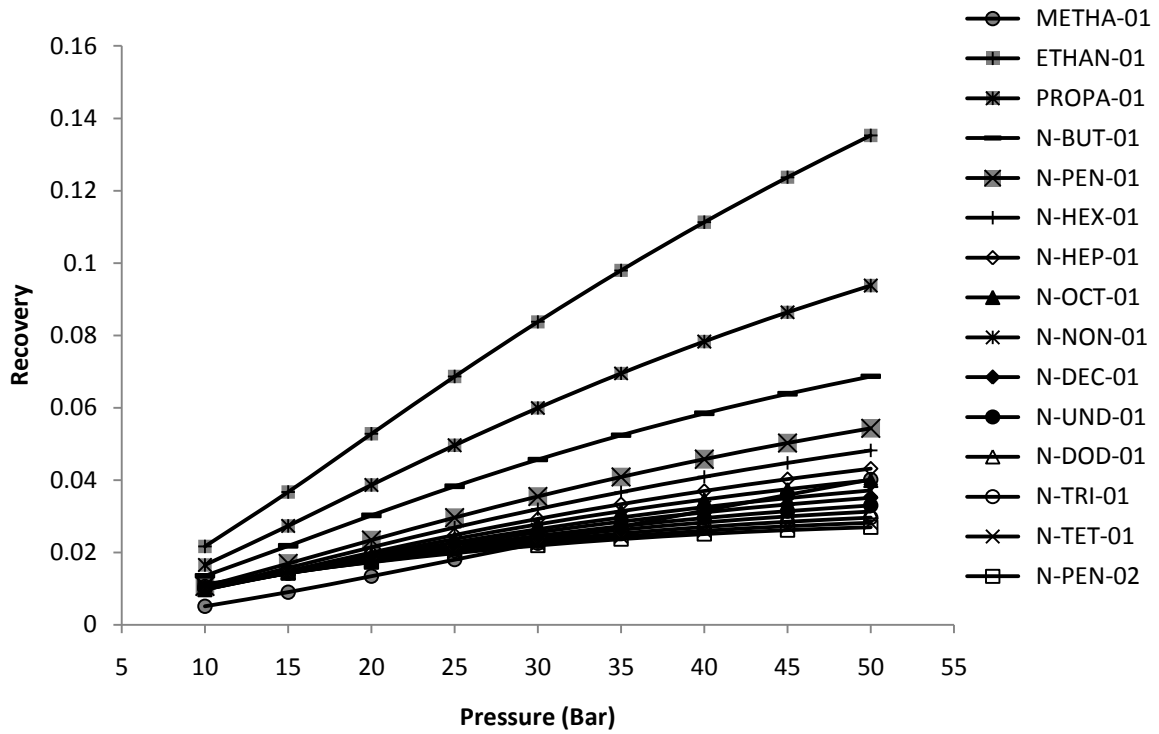

Figure 22: Predicted recovery of hydrocarbons to the liquid stream in a flash unit using the UNIFAC model at 180˚C.

5.3.2 Equilibrium distribution for hydrocarbons

Figure 23 shows a graph of the predicted equilibrium K-values at 180˚C and a pressure range of 10–50 bar. These results were obtained using the NTRL thermodynamic property model. The trend of the equilibrium K-value for C_1-C_3 hydrocarbons is similar to the trend of the water equilibrium K-value in Figure 13. Figure 23 suggests that at 10 bar there would be more C_1–C_3 hydrocarbons in the vapour stream than in the liquid stream. However, the amounts of these

hydrocarbons would decrease with increased pressure. A comparison of the plots of the theoretical calculated K-values and the simulated K-values shows that the difference between them decreases with increasing pressure and the theoretical K-values approach the simulated K-values.

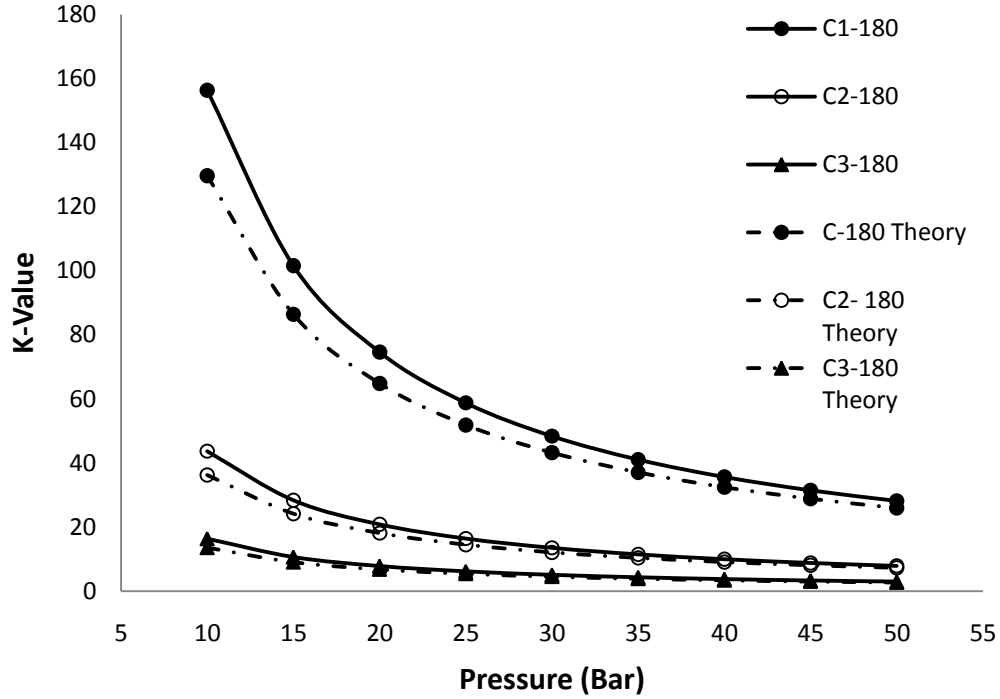

Figure 23: Predicted K-values for C_1–C_3 hydrocarbons at 180˚C obtained using the NTRL model compared to predicted K-values using Raoult's law

Figure B2.13 in Appendix B2 represents the equilibrium K-value for C_4-C_6 hydrocarbons; the trend is different from that of C_1–C_3.The difference is that the equilibrium K-value for C_4-C_6 does not decrease with hydrocarbon carbon number, as it does for C_1-C_3, but the equilibrium K-value still decreases with an increase in pressure. The equilibrium K-values in Figures B2.13 and B2.14 generally decrease with increasing carbon number at a pressures above 20 bar. The equilibrium K-values of C_7-C_{10} hydrocarbons shows that these hydrocarbons

will be more concentrated in the liquid phase than in the vapour phase. The equilibrium K-values of decane is 0.988 at a pressure of 10 bar and 0.390 at 50 bar. This equilibrium K-value of less than 1 suggests that decane will predominantly appear in the liquid phase rather than in the vapour phase.

Figure 24 shows the equilibrium K-values of C_{11}–C_{15} hydrocarbons, which follow the same trend as that of C_1–C_3 hydrocarbons in Figure 23. The maximum K-values for these hydrocarbons is 0.269 for C_{11} at 10 bar; all the other hydrocarbons have a value less than 0.269, which implies that these hydrocarbons predominantly report to the liquid phase.

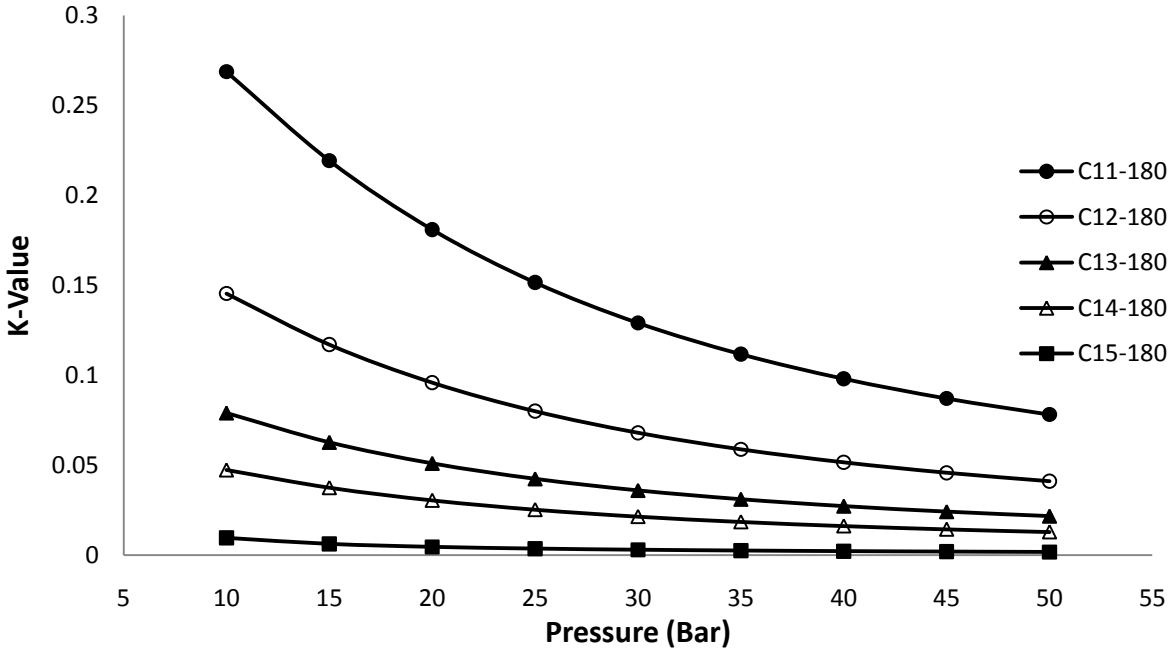

Figure 24: Predicted K-values for C_{11}-C_{15} hydrocarbons at 180˚C using the NTRL thermodynamic model

5.4 Results of water recovery process simulation using glycerol for the glycerol recycle system

Figure 25 shows the overall mass balance of the process simulation with a recycle stream. The simulation results show that 90% of water is removed from the system when a total molar flow rate of 90 kmol/s of glycerol is fed into the absorber unit. The amount of glycerol recycled in the process is about 86.35 kmol/s, and about 3.65 kmol/s of glycerol is fed to make up for the lost glycerol.

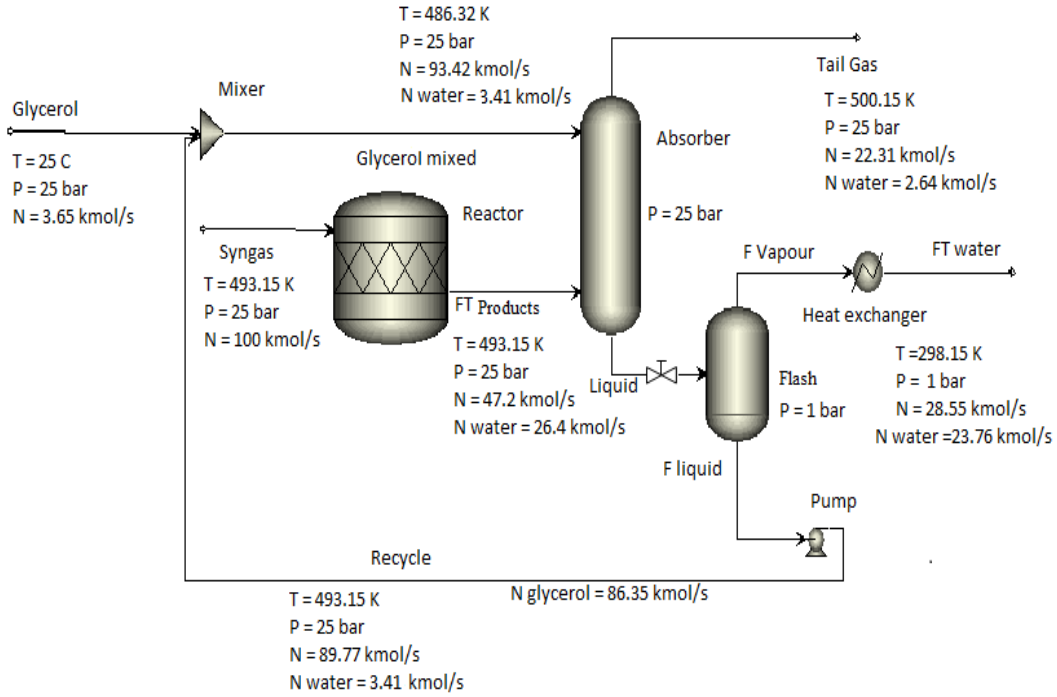

Figure 25: Mass balance of process simulation at 90% water removal

Glycerol contains about 3.8% of water of which reduces the ability of glycerol to absorb The recycled water in the process. Recycling glycerol in the process does not improve the recovery of water, but reduces the amount of fresh feed glycerol needed to remove the same amount of water in the process.

Figure 26 represents the results obtained from performing a sensitivity study to investigate the effect of glycerol (feed) flow rate at different temperatures. The results show that at a low temperature (25˚C), about 30 kmol/s (26.4 kmol/s) of glycerol is needed to completely remove water produced from the FT product stream.

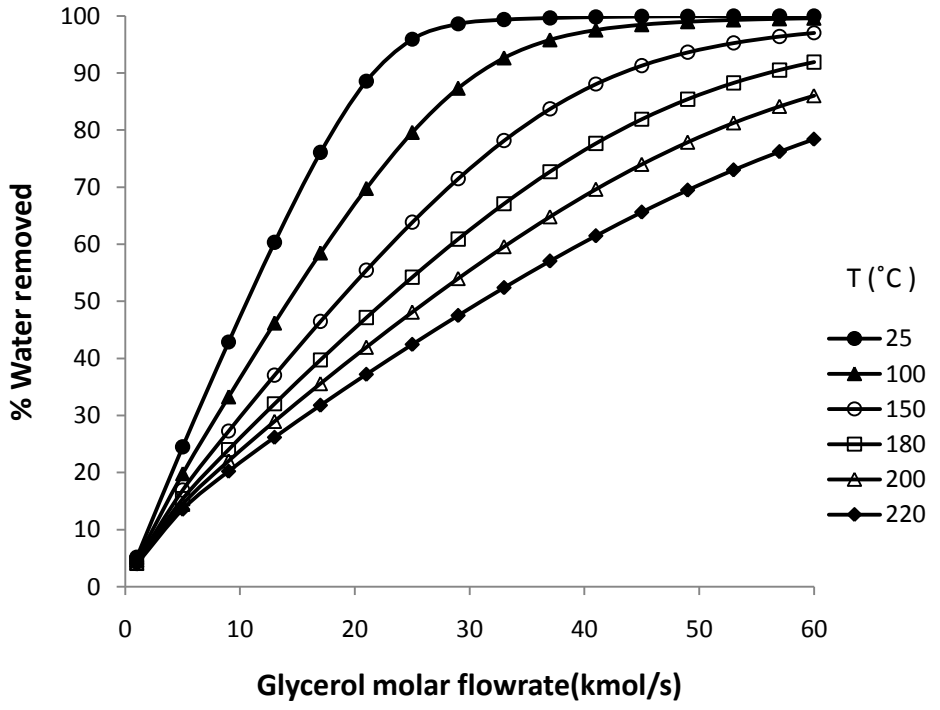

Figure 26: Sensitivity study of glycerol feed flow rate at various temperatures using the NTRL model at 10 bar

However, as the feed temperature of glycerol increases, more glycerol is needed to remove more water from the tail gas stream. When glycerol is fed at 150˚C, the amount of glycerol needed to completely remove water is about 60 kmol/s, which is twice the amount needed to completely remove water when the glycerol feed temperature is 25˚C. When the glycerol feed temperature is above 150˚C, flow rates greater than 60 kmol/s will be required because only 85% and less of water

is removed. Refer to Appendix B3 for Aspen results, including all other process variables.

Table B3.1 in Appendix B3 shows detailed results of the process simulation. The liquid stream from the absorber contains 0.76 molar fraction of glycerol, while the mole fraction of water is about 0.23. On a mass basis, the liquid stream contains 94% glycerol and 6% water, which suggests that glycerol on a molar basis absorbs more moles of water, but on a mass basis more glycerol is needed to absorb water.

The tail gas stream exits the process at about 227˚C and at this temperature the tail gas stream does not need further heating for it to be sent into a secondary reactor for further reaction. Figure 27 shows the effect of glycerol feed temperature on the tail gas stream temperature; when the feed temperature of glycerol is increased, the temperature of the tail gas stream also increases. This has a negative impact on the amount of water removed from the tail gas stream: if the glycerol feed temperature is high, less water is removed by glycerol, and this leaves more water in the tail gas stream.

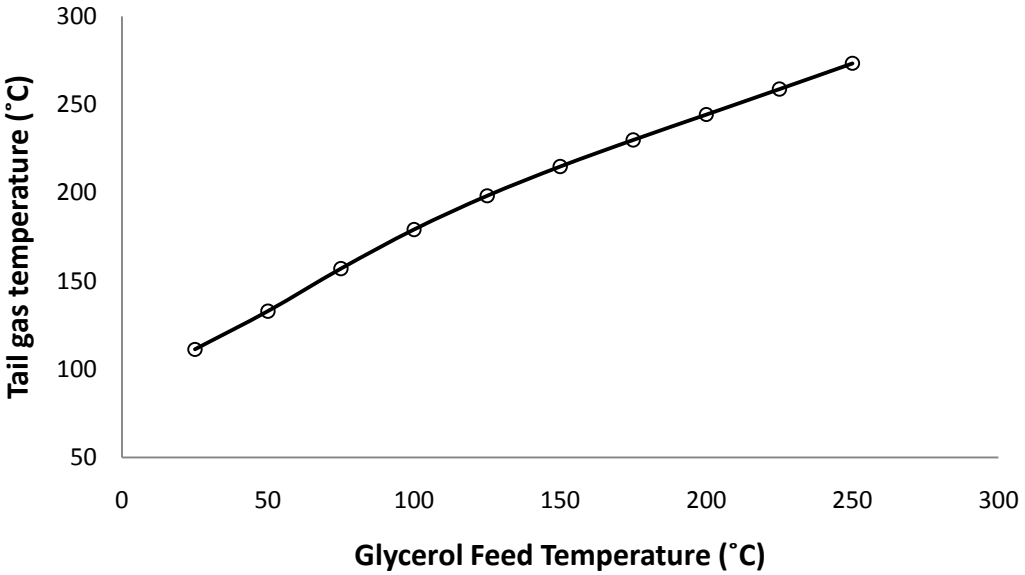

Figure 27: Effect of glycerol feed temperature on tail gas stream temperature

The FT water stream contains about 83% water, 12% glycerol and 5% hydrocarbons, which can be separated at the cold separation plant by distillation. However, the separation of the glycerol-water system has cost implications.

5.5 Concluding remarks

This chapter presents results obtained from Aspen simulations, which show that glycerol can remove water from the FT product stream; the extent of the removal depends on three parameters, namely pressure, temperature and glycerol flow rate. Water removal increased with pressure at a specific temperature and decreased with increasing temperature at a specific pressure. It was also found that water

removal increased with an increasing molar flow rate of glycerol, which suggests that the increase was due to an increase in the molar ratio of glycerol to water.

The amount of hydrocarbons that were removed by glycerol with water, were found to be in trace quantities relative to water at 10 bars and 180 °C and the influence of pressure and temperature was found to be the same as that of water removal. However, the glycerol flow rate had no significant effect on the recovery of hydrocarbons. The NTRL and UNIQUAC thermodynamic property models were found to predict the same behaviour. There were, however, minor differences in the numeric data of these simulations, which may be a result of the inaccuracy of these models. The UNIFAC model was not adequate in predicting the results because of limitation under which the model may be used. Due to a lack of experimental data for such a process, one cannot comment much on the accuracy, but the results obtained from NTRL and UNIQUAC models were in agreement. Comparing the VLE model results for water and glycerol showed that NTRL was a better model than UNIQUAC.

CHAPTER 6

CONCLUSIONS AND OUTLOOK

6.1 The approach

The purpose of the dissertation was to develop a method of removing water from a hydrocarbon product stream of the FT reactor operating under commercial FT conditions. The focal point of this dissertation was to decrease the concentration of water from the reactor product stream by adding a liquid phase as an absorbent. The liquid absorbent used had to be hygroscopic and immiscible with the hydrocarbon products produced in the FT process. After water has been removed from the reactor product stream, the water-reduced reactor product stream would then be returned to the reactor in order to improve the overall conversion of the Fischer-Tropsch reaction. The overall product removal from the FT process usually occurs by purging a reactor product stream to the separation plant via a series of distillation columns.

6.2 Summary of main results

Simulation results from Aspen were used to assess the proposed process of removing water from the FT product stream. Water removal from the FT product stream is defined as the ability to remove water contained in the FT products. The

general outcomes of the simulation process was that water removal increased with pressure at a constant temperature and also that the amount of water removed by glycerol decreased with temperature at constant pressure.

The glycerol water-removal process requires cooling of only the separated water stream, whereas the traditional knock-out method requires cooling and heating. The amount of energy required by the glycerol water-removal process is low compared to the knock-out process, which suggests that the glycerol water removal can be more energy efficient than the knock-out process.

6.3 Recommendations

This work presents a conceptual and theoretical study of water removal from the Fischer-Tropsch product stream by exploiting the hygroscopic property of liquid glycerol. Further work should focus on conducting experiments that will provide the opportunity to consider the practicalities associated with the glycerol water-removal process and further validate the simulation results and the viability of the process.

References

1. Dry, M., “The Fischer–Tropsch process: 1950–2000”, Catalysis Today, 71, 2002, pp.227–241.

2. Dry, M., “Fischer–Tropsch reactions and the environment”, Applied Catalysis, 189, 1999, pp. 185–190.

3. Rostrup-Nielsen, J. R., “Syngas in perspective”, Catalysis Today, 71, 2002, pp. 243–247.

4. Bartholomew, C .H., “Recent technological developments in Fischer-Tropsch catalysis”, Catalysis Letters,7,1990, pp. 303–316

5. Luo, M., Hamdeh, H., Davis, H.B., “Fischer-Tropsch synthesis catalyst activation of low alpha iron catalyst”, Catalysis Today,140, 2009, pp.127–134.

6. Rothaemel, M., Hanssen, K.F., Blekkan, A.E., Schanke, D., Holmen A., “The effect of water on cobalt Fischer-Tropsch catalysts studied by steady-state isotopic transient kinetic analysis”, Catalysis Today, 38, 1997, pp.79–84.

7. Botes, F.G., “Influences of water and syngas partial pressure on the Kinetics of a commercial Alumina-Supported Cobalt Fischer-Tropsch catalyst”, Ind. Eng. Chem. Res, 48, 2009, pp.1859–1865.

8. Satterfleid, N.C., Hanlon, R.T., “Effect of water on the Iron-catalyzed Fischer-Tropsch synthesis”, Ind. Eng. Chem. Prod. Res. Dev, 25,1986, pp. 407–414.

9. Pour, A.N., Shahri, S.M.K., Zamani, Y., Irani, M., Tehrani, S., “Deactivation studies of bifunctional Fe-HZSM5 catalyst in Fischer-Tropsch process”, Journal of Natural Gas Chemistry,17,2008, pp. 242–248.

10. Li, J., Jacobs, G., Das, T., Zhang, Y., Davis, B., “Fischer–Tropsch synthesis: effect of water on the catalytic properties of a Co/SiO_2 catalyst”, Applied Catalysis A: General, 236, 2002, pp. 67–76.

11. Jacobs, G., Patterson, M.P., Das, T.K., Luo, M. Davis, H.B., “Fischer–Tropsch synthesis: effect of water on Co/Al2O3 catalysts and XAFS characterization of reoxidation phenomena”, Applied Catalysis A: General, 270, 2004, pp. 65–76.

12. Krishna, R. and Sie , S.T., “Design and scale-up of the Fischer-Tropsch bubble column slurry reactor”, Fuel Processing Technology, 64, 2000, pp.73–105.

13. Rousseau, I. and Ronald, W., Separation Technology-Handbooks, John Wiley & Sons, Inc., New York, 1987.

14. Hoogendoorn, J.C. and Salomon, J.M., “Sasol: Largest oil-from-coal plant”, British Chem.Eng. 1957, June, 308.

15. De Klerk, A., “Fuels refining in the future: Sasol technology”, Technology conference: Sasolburg ,South Africa, 2005 (13 October).

16. Bestani, B. and Shing, K.S., “Infinite-Dilution Activity Coefficients of Water in TEG, PEG, Glycerol and their Mixtures in the Temperature Range 50˚C to 140˚C”, Fluid Phase Equilibria, 50, 1989, pp. 209–221.

17. Soujanya, J., Satyavathi,B., Vittal Prasad,T.E., “Experimental (vapour + liquid) equilibrium data of (methanol + water), (water + glycerol) and (methanol + glycerol) systems at atmospheric and sub-atmospheric pressures”, J. Chem. Thermodynamics, 42, 2010, pp. 621–624.

Appendix A

Table A1: True coefficient of thermal conductivity of glycerol-water solutions (adapted from Glycerin Producers Association, 1969)

Water	Glycerol										Equation for true coefficient of thermal conductivity
% by weight		10	20	30	40	50	60	70	80	$\propto_{20}$ %,	$\propto$ *is defined by* $k_t = k_t + [1 + \propto_{20} (t - 20)]$
		Gram	Calories,	Second^{-1}	,cm^{-2}	,$^{\circ}$C^{-1}	,cm			$^{\circ}$C^{-1}	
100	Pure water	0.00138	0.00141	0.00145	0.00149	0.00152	0.00156	0.0016	0.00163	0.26	$k_t = 0.00134 + 0.00000367\ (t)$
95	5	0.00133	0.00137	0.0014	0.00144	0.00147	0.00151	0.00154	0.00158	0.25	$k_t = 0.00130 + 0.00000342(t)$
90	10	0.0013	0.00133	0.00137	0.0014	0.00143	0.00146	0.00149	0.00152	0.24	$k_t = 0.00127 + 0.00000317(t)$
85	15	0.00125	0.00128	0.00131	0.00134	0.00137	0.0014	0.00143	0.00146	0.23	$k_t = 0.00122 + 0.00000300(t)$
80	20	0.00121	0.00124	0.00127	0.00129	0.00132	0.00135	0.00138	0.00141	0.23	$k_t = 0.00118 + 0.00000284(t)$
75	25	0.00117	0.00119	0.00122	0.00125	0.00127	0.0013	0.00132	0.00135	0.22	$k_t = 0.00114 + 0.00000263(t)$
70	30	0.00112	0.00115	0.00117	0.0012	0.00122	0.00124	0.00126	0.00129	0.2	$k_t = 0.00110 + 0.00000234(t)$
65	35	0.00109	0.00111	0.00114	0.00116	0.00118	0.0012	0.00122	0.00124	0.2	$k_t = 0.00107 + 0.00000217(t)$
60	40	0.00105	0.00107	0.00108	0.0011	0.00112	0.00114	0.00116	0.00118	0.17	$k_t = 0.00103 + 0.00000183(t)$
55	45	0.00102	0.00103	0.00105	0.00106	0.00108	0.0011	0.00111	0.00113	0.15	$k_t = 0.00100 + 0.00000159(t)$
50	50	0.00097	0.00099	0.001	0.00101	0.00103	0.00104	0.00105	0.00107	0.13	$k_t = 0.00096 + 0.00000133(t)$
45	55	0.00094	0.00095	0.00096	0.00098	0.00099	0.001	0.00101	0.00102	0.12	$k_t = 0.00093 + 0.00000116(t)$

40	60	0.0009	0.00091	0.00091	0.00092	0.00093	0.00094	0.00095	0.00096	0.1	$k_t = 0.00089 + 0.000000090(t)$
35	65	0.00086	0.00087	0.00088	0.00089	0.00089	0.0009	0.00091	0.00091	0.08	$k_t = 0.00083 + 0.00000067(t)$
30	70	0.00084	0.00084	0.00085	0.00085	0.00086	0.00086	0.00087	0.00087	0.06	$k_t = 0.00080 + 0.00000050(t)$
25	75	0.0008	0.00081	0.00081	0.00081	0.00082	0.00082	0.00082	0.00082	0.04	$k_t = 0.00077 + 0.00000030(t)$
20	80	0.00077	0.00078	0.00078	0.00078	0.00079	0.00079	0.00079	0.00079	0.04	$k_t = 0.00074 + 0.00000030(t)$
15	85	0.00074	0.00074	0.00074	0.00074	0.00074	0.00074	0.00075	0.00075	0.01	$k_t = 0.00072$
10	90	0.00072	0.00072	0.00072	0.00072	0.00072	0.00072	0.00072	0.00073		$k_t = 0.00072$
5	95	0.0007	0.0007	0.0007	0.0007	0.0007	0.0007	0.0007	0.0007		$k_t = 0.00070$
Pure glycerol	100	0.00068	0.00068	0.00068	0.00068	0.00068	0.00068	0.00068	0.00068		$k_t = 0.00068$

Table A2: Experimental T–x values and derived phase equilibrium information of water (1) + glycerol (2) binary system at various pressures. (Soujanya et al., 2009)

				P = 14.19 kPa					P = 29.38 kPa
x1	x2	y1	y2	T(k)	1	0	1	0.00E+00	341.8
1	0	1	0.00E+00	326.1	0.95	0.05	0.999999	1.00E-06	343
0.95	0.05	1	0.00E+00	327.1	0.8	0.2	0.999992	8.00E-06	347.4
0.9	0.1	0.999999	1.00E-06	328.35	0.7	0.3	0.999981	1.90E-05	351.2
0.8	0.2	0.999998	2.00E-06	331.35	0.6	0.4	0.999957	4.30E-05	356.15
0.7	0.3	0.999994	6.00E-06	335.15	0.5	0.5	0.999902	9.80E-05	361.85
0.6	0.4	0.999986	1.40E-05	339.9	0.4	0.6	0.99976	2.40E-04	369.4
0.5	0.5	0.999961	3.90E-05	346	0.3	0.7	0.999336	6.64E-04	379.5
0.4	0.6	0.999889	1.11E-04	353.75	0.2	0.8	0.997656	2.34E-03	394.4
0.3	0.7	0.999629	3.71E-04	364.3	0.1	0.9	0.985615	1.44E-02	421.1
0.2	0.8	0.998392	1.61E-03	379.65	0	1	0	1.00E+00	519.05
0.1	0.9	0.98748	1.25E-02	406.7					
0	1	0	1.00E+00	497.1					
				P = 41.54 kPa					P = 54.72 kPa
1	0	1	0.00E+00	349.95	1	0	1	0.00E+00	356.7
0.95	0.05	0.999999	1.00E-06	351.2	0.95	0.05	0.999998	2.00E-06	358.15
0.9	0.1	0.999997	3.00E-06	352.7	0.9	0.1	0.999995	5.00E-06	359.6
0.8	0.2	0.999989	1.10E-05	356.25	0.8	0.2	0.999983	1.70E-05	363.25
0.7	0.3	0.999973	2.70E-05	360.7	0.7	0.3	0.999959	4.10E-05	367.8
0.6	0.4	0.999932	6.80E-05	366.35	0.6	0.4	0.999901	9.90E-05	373.5
0.5	0.5	0.999827	1.73E-04	373.55	0.5	0.5	0.999761	2.39E-04	380.7

0.4	0.6	0.99953	4.70E-04	382.85	0.4	0.6	0.999379	6.21E-04	390.1
0.3	0.7	0.998542	1.46E-03	395.4	0.3	0.7	0.998169	1.83E-03	402.8
0.2	0.8	0.994207	5.79E-03	414.1	0.2	0.8	0.99321	6.79E-03	421.45
0.1	0.9	0.961908	3.81E-02	446.5	0.1	0.9	0.958629	4.14E-02	454.15
0	1	0	1.00E+00	530.4	0	1	0	1.00E+00	540
				P = 63.84 kPa					P = 95.3 kPa
1	0	1	0.00E+00	360.65	1	0	1	0.00E+00	371.45
0.9	0.1	0.999996	4.00E-06	363.8	0.95	0.05	0.999996	4.00E-06	373
0.8	0.2	0.999986	1.40E-05	368.05	0.9	0.1	0.99999	1.00E-05	374.6
0.7	0.3	0.999958	4.20E-05	373.6	0.8	0.2	0.999969	3.10E-05	378.7
0.6	0.4	0.999882	1.18E-04	380.75	0.7	0.3	0.999921	7.90E-05	383.9
0.5	0.5	0.999657	3.43E-04	390	0.6	0.4	0.999808	1.92E-04	390.55
0.4	0.6	0.998917	1.08E-03	402.25	0.5	0.5	0.999518	4.82E-04	399.1
0.3	0.7	0.996046	3.95E-03	419.1	0.4	0.6	0.998694	1.31E-03	410.35
0.2	0.8	0.981776	1.82E-02	443.85	0.3	0.7	0.995958	4.04E-03	425.8
0.1	0.9	0.876663	1.23E-01	484.4	0.2	0.8	0.984275	1.57E-02	448.7
0	1	0	1.00E+00	545.6	0.1	0.9	0.906723	9.33E-02	487.5
					0	1	0	1.00E+00	560.8

X1 is the water mole fraction in liquid phase, X2 is glycerol mole fraction in liquid phase,Y1 is the water mole fraction in vapour phase, Y2 is glycerol mole fraction in vapour phase

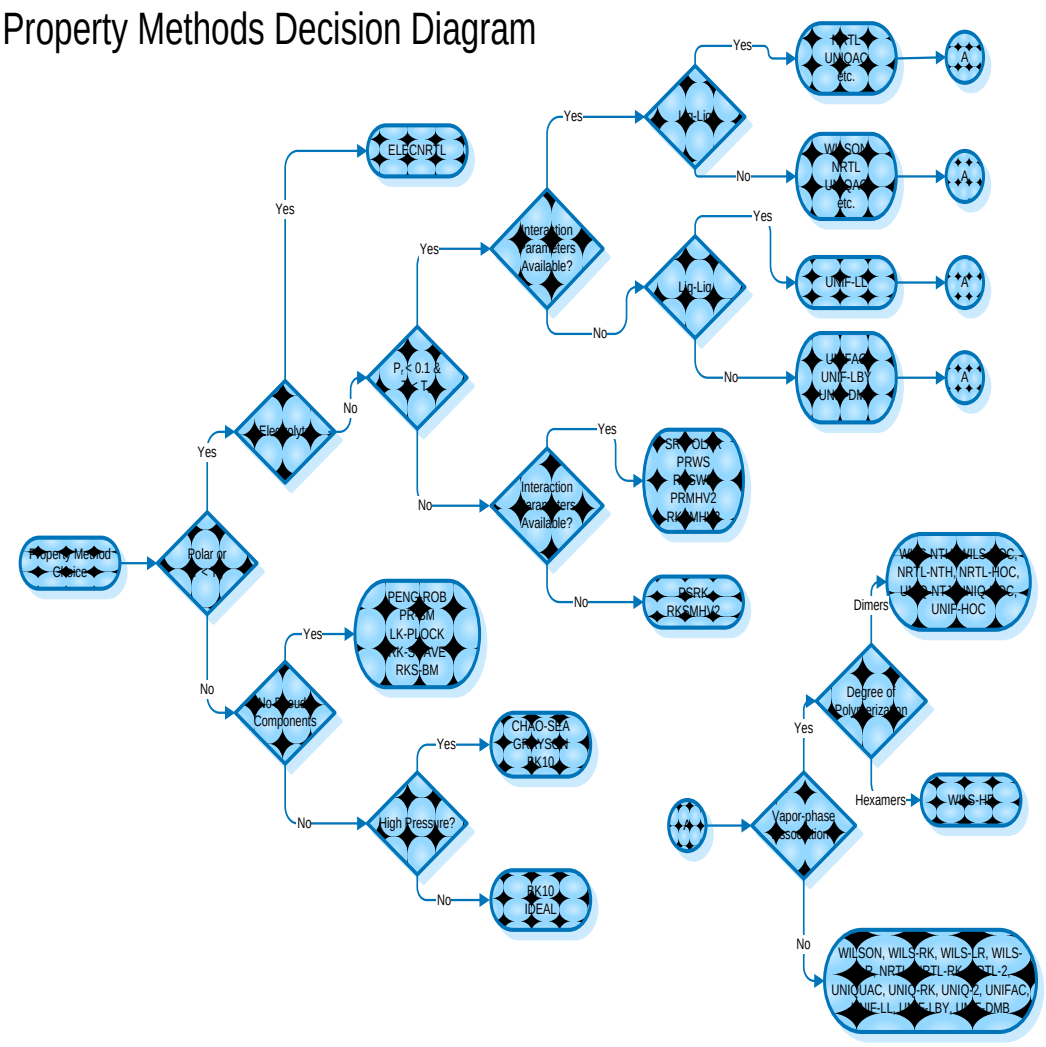

Figure A 1: Assistant for selecting a property method

Appendix B

Appendix B1: Water equilibrium constant results

Tables B1.1 to B1.3 show the K-values of water at various temperatures and pressures for the NTRL, UNIQUAC and UNIFAC property models.

Table B1. 1: NTRL K-values of water

T (°C)	Pressure (bar)								
	10	15	20	25	30	35	40	45	50
180	0.815733	0.580555	0.448823	0.365271	0.307813	0.265954	0.234123	0.209115	0.188941
200	1.12829	0.830891	0.656965	0.541817	0.460256	0.399705	0.353089	0.316148	0.286176
220	1.477315	1.112337	0.899551	0.755373	0.650092	0.569769	0.506594	0.455723	0.413959
240	1.866914	1.42019	1.164964	0.993229	0.866908	0.768858	0.690191	0.625583	0.571621
260	2.302104	1.756805	1.451197	1.248502	1.100692	0.986214	0.893897	0.817355	0.752569
280	2.785614	2.125307	1.760153	1.521139	1.348683	1.216271	1.110092	1.022224	0.947779
300	3.316317	2.526943	2.093837	1.812736	1.611801	1.458707	1.336841	1.236611	1.152092

Table B1.2: UNIQUAC K-values of water

T (°C)	Pressure (bar)								
	10	15	20	25	30	35	40	45	50
180	0.771842	0.550424	0.427694	0.350045	0.296663	0.257772	0.228178	0.204891	0.18608
200	1.068974	0.782812	0.61956	0.512635	0.437238	0.381367	0.338385	0.304323	0.276692
220	1.411548	1.049771	0.845446	0.709767	0.61188	0.53771	0.479603	0.432912	0.394634
240	1.806947	1.350706	1.098749	0.933177	0.813447	0.721709	0.648749	0.589212	0.539692
260	2.262615	1.690312	1.380098	1.179436	1.035869	0.926336	0.839074	0.767412	0.707257
280	2.784232	2.073356	1.693065	1.450187	1.278416	1.148614	1.045898	0.961841	0.891304
300	3.376002	2.503241	2.040854	1.748227	1.543093	1.389413	1.268732	1.17063	1.08874

Table B1.3: UNIFAC K-values of water

T (°C)	Pressure (bar)								
	10	15	20	25	30	35	40	45	50
180	1.044293	0.714653	0.548749	0.448904	0.3823	0.334752	0.299144	0.271502	0.249443
200	1.579187	1.079446	0.828488	0.677191	0.576012	0.503643	0.449358	0.407162	0.373453
220	2.287116	1.560266	1.196342	0.977361	0.83088	0.725945	0.647087	0.585695	0.53657
240	3.186136	2.169484	1.660997	1.355593	1.151644	1.005655	0.89593	0.810427	0.741929
260	4.286151	2.91392	2.227717	1.815866	1.541084	1.344742	1.197279	1.082444	0.990469
280	5.584861	3.791968	2.895333	2.357259	1.998508	1.742195	1.549896	1.400281	1.28053
300	7.062902	4.791001	3.654428	2.972297	2.517507	2.192645	1.948996	1.759509	1.607923

Appendix B2: Hydrocarbon recovery results

Figures B2.1 to B2.15 show the hydrocarbon recovery results at various temperatures and pressures for the NTRL, UNIQUAC and UNIFAC property models.

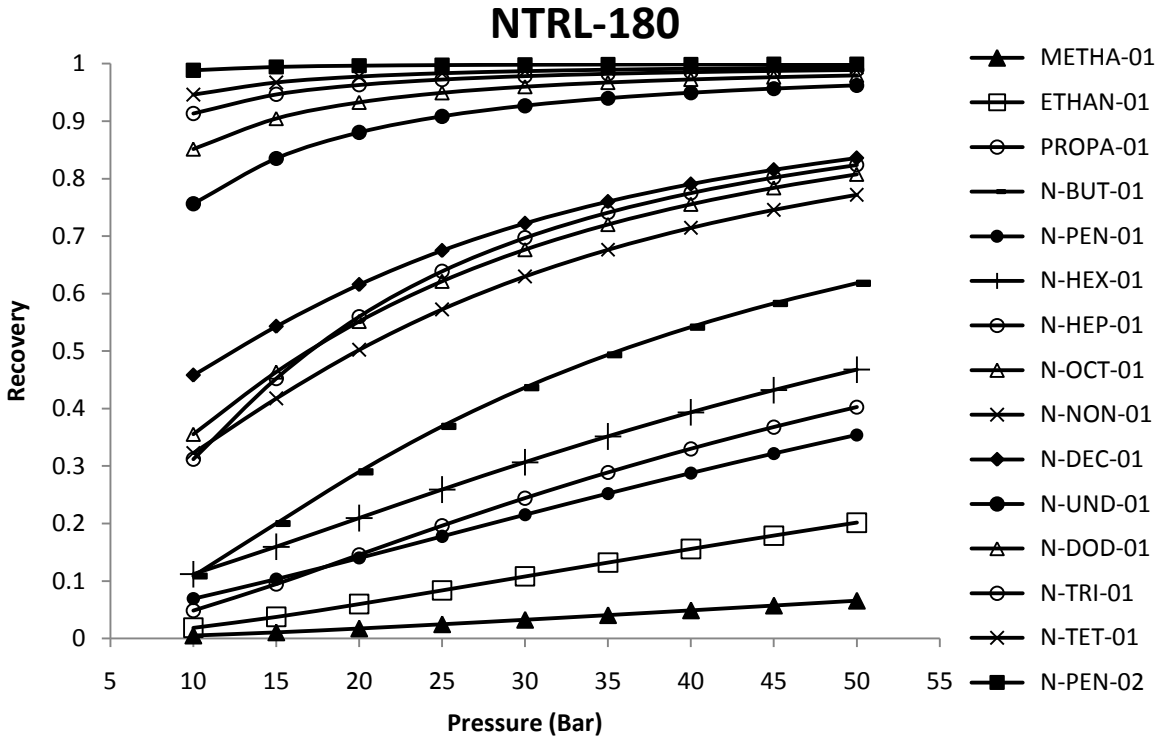

Figure B2. 1: NTRL model recovery results for hydrocarbons at 180˚C

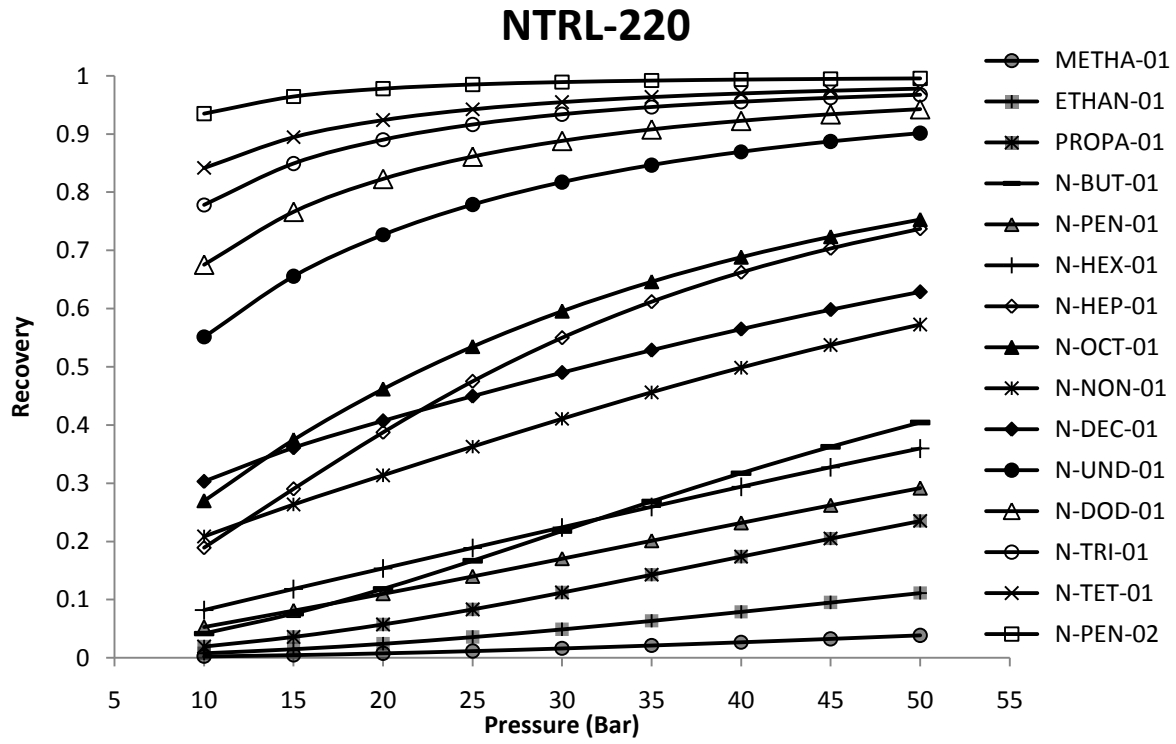

Figure B2. 2: NTRL model recovery results for hydrocarbons at 220˚C

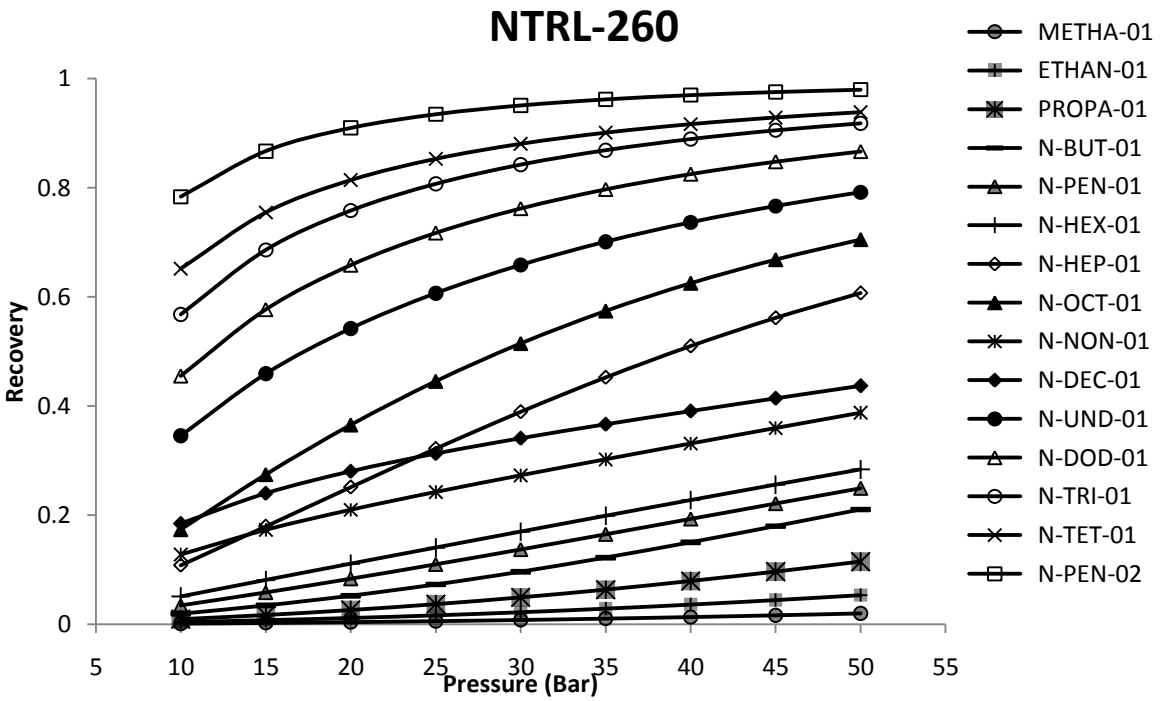

Figure B2. 3: NTRL model recovery results for hydrocarbons at 260˚C

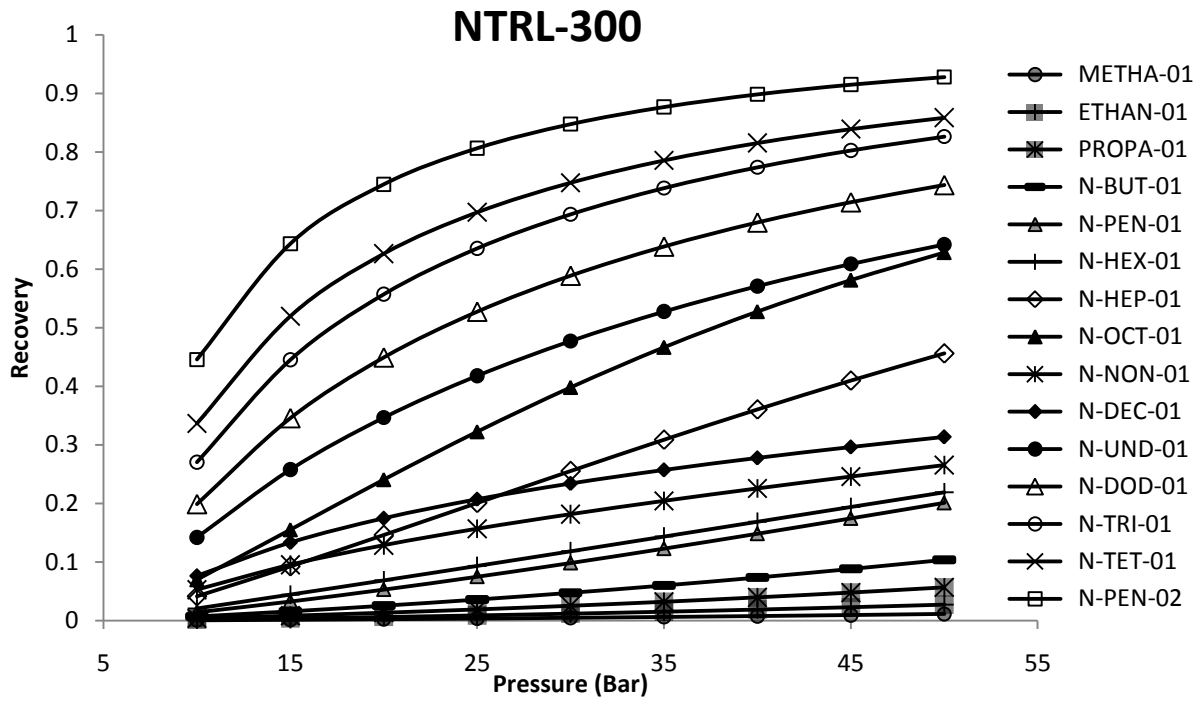

Figure B2. 4: NTRL model recovery results for hydrocarbons at 300˚C

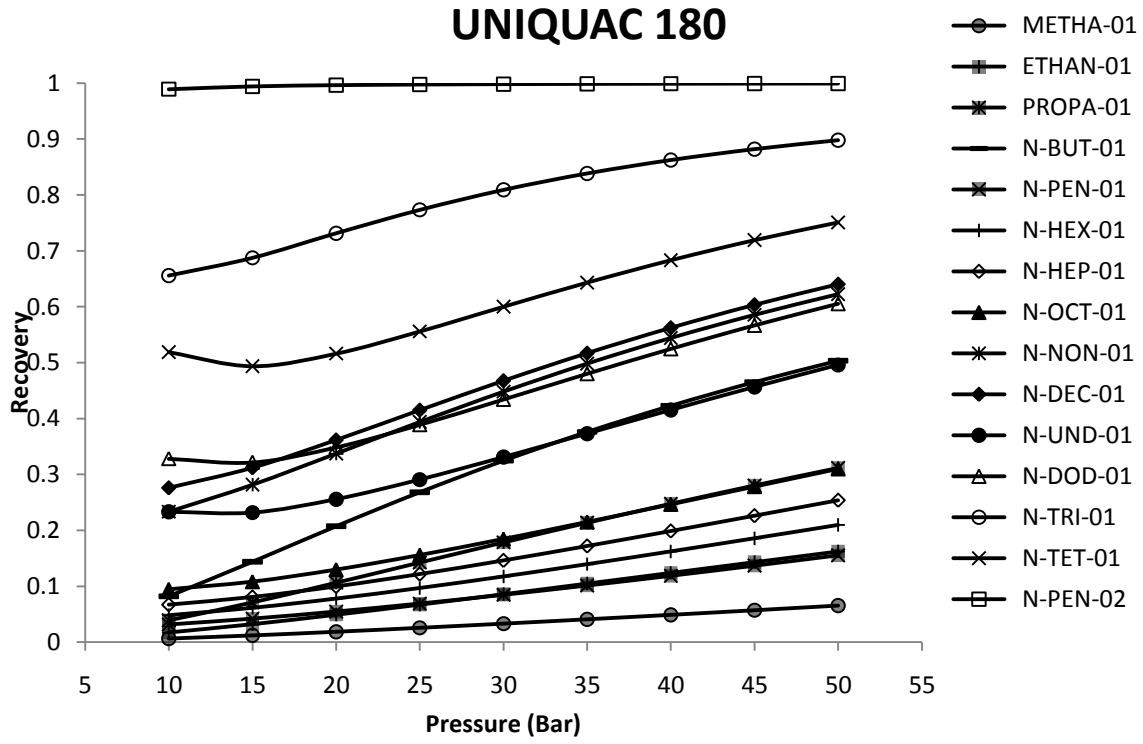

Figure B2. 5: UNIQUAC model recovery results for hydrocarbons at 180˚C

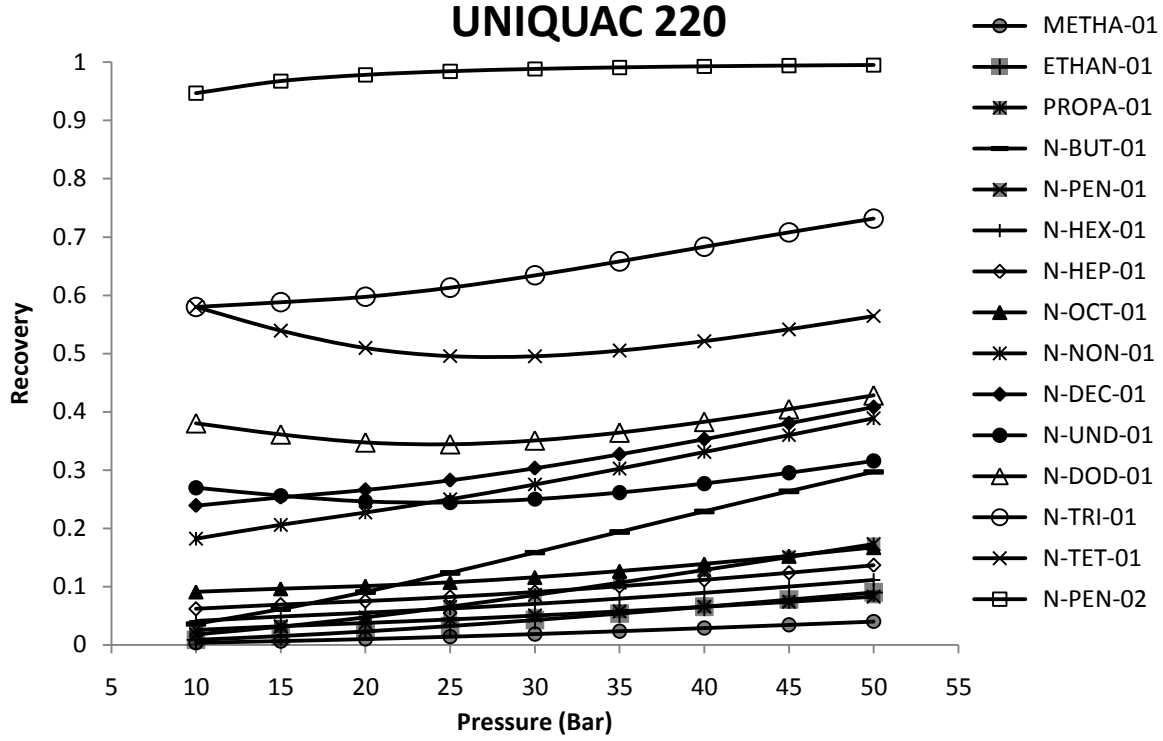

Figure B2. 6: UNIQUAC model recovery results for hydrocarbons at 220˚C

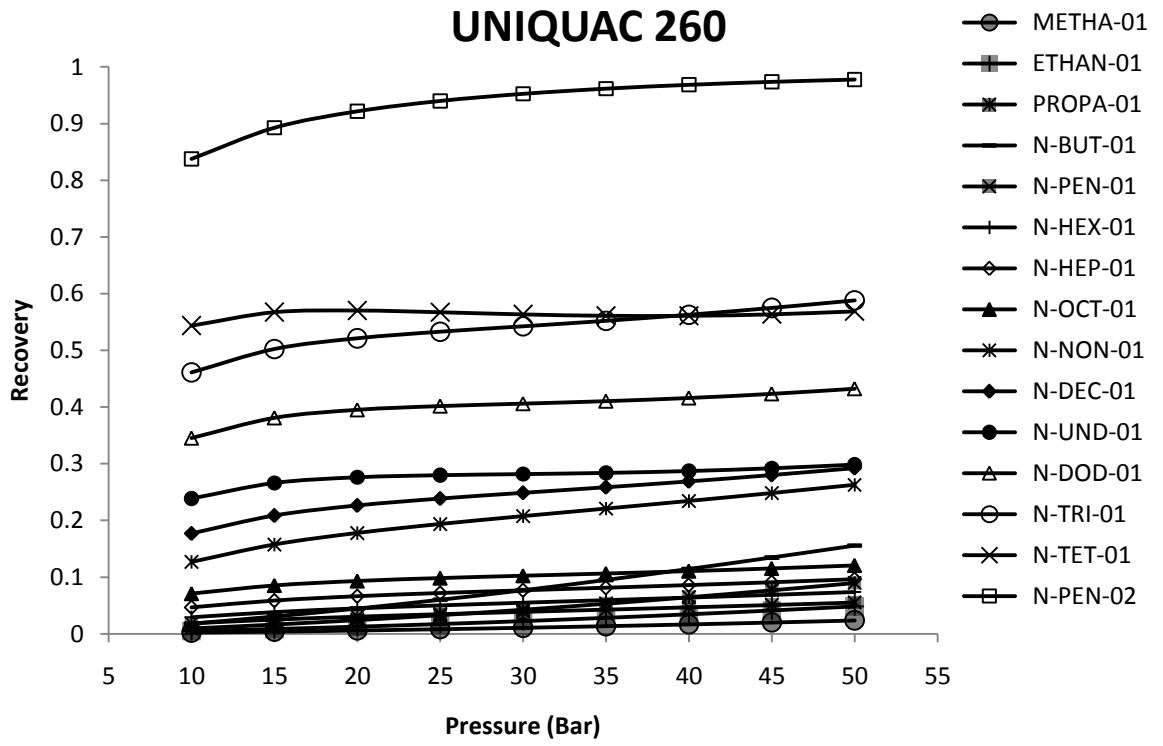

Figure B2. 7: UNIQUAC model recovery results for hydrocarbons at 260˚C

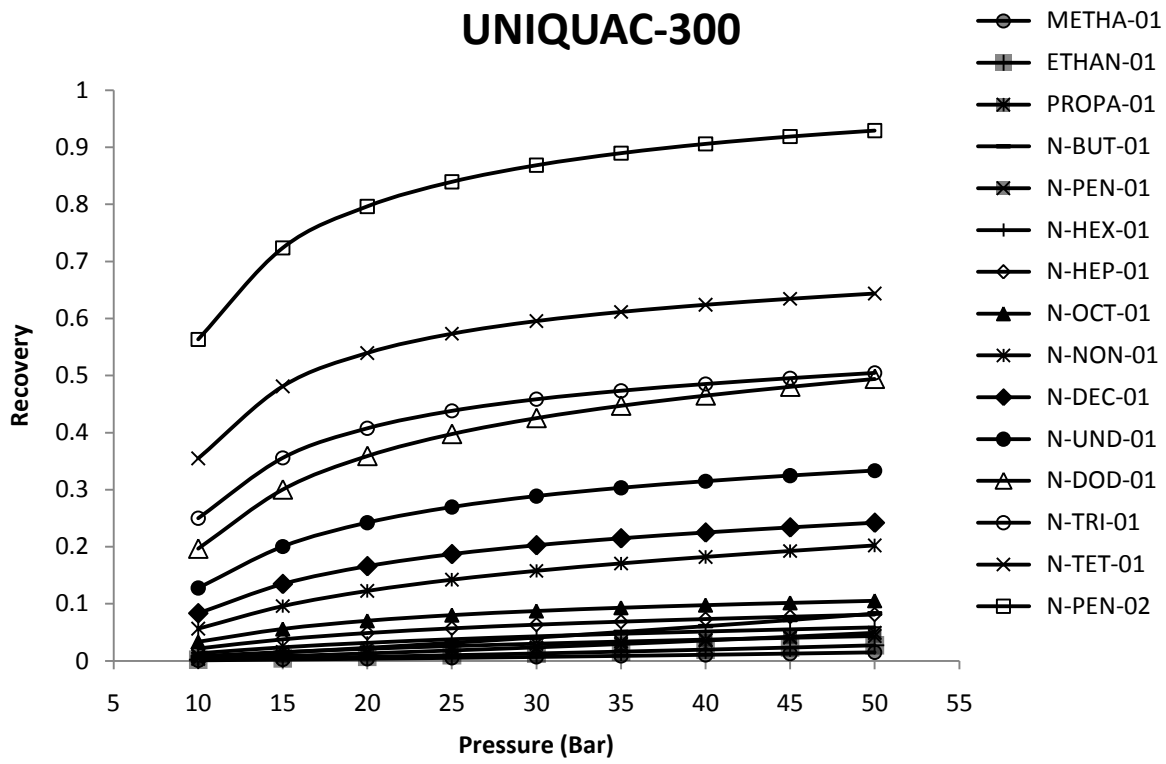

Figure B2. 8: UNIQUAC model recovery results for hydrocarbons at 300˚C

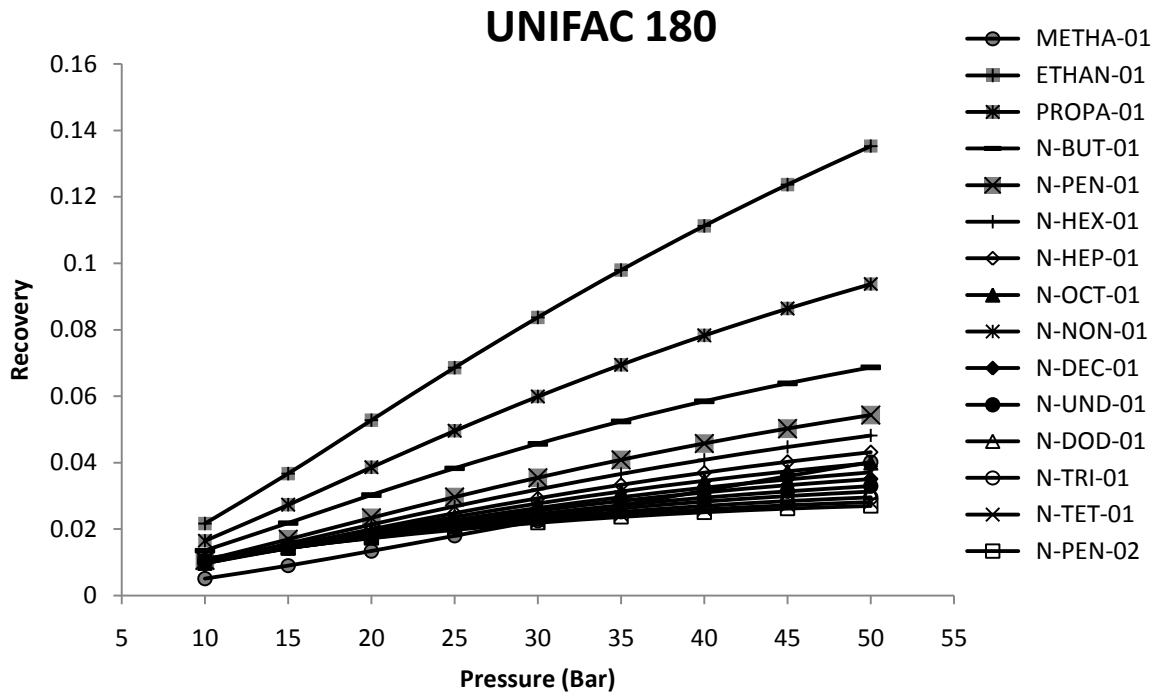

Figure B2. 9: UNIFAC model recovery results for hydrocarbons at 180˚C

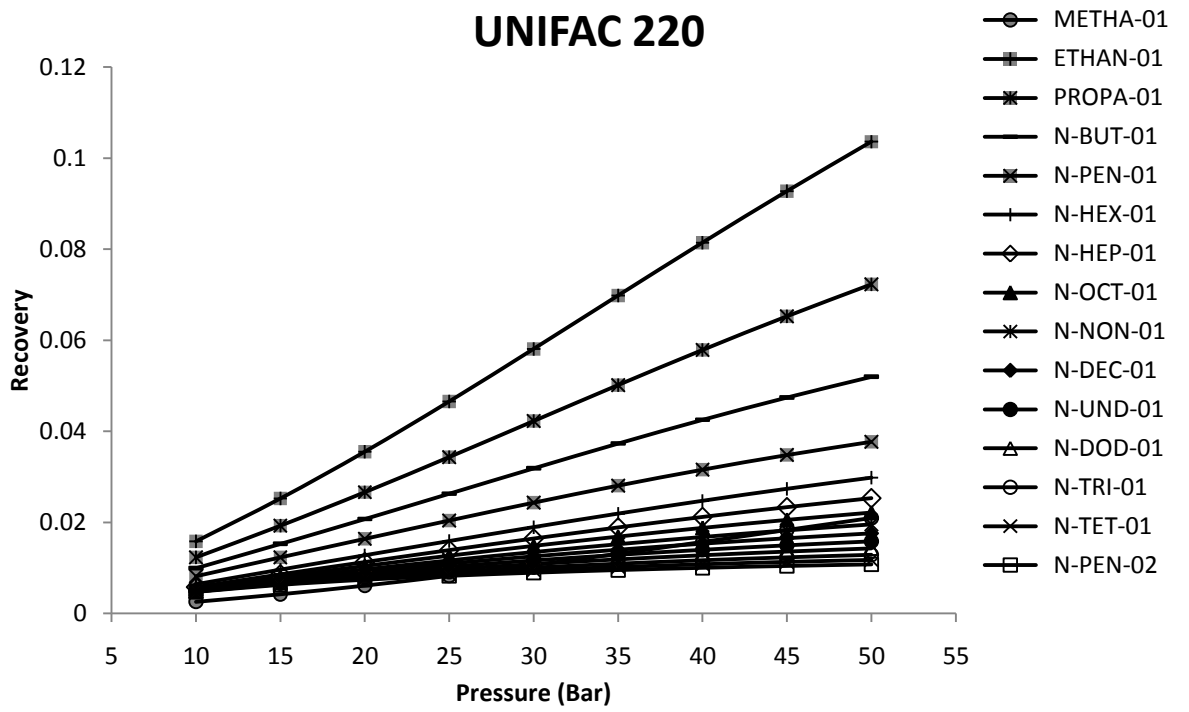

Figure B2. 10: UNIFAC model recovery results for hydrocarbons at 220˚C

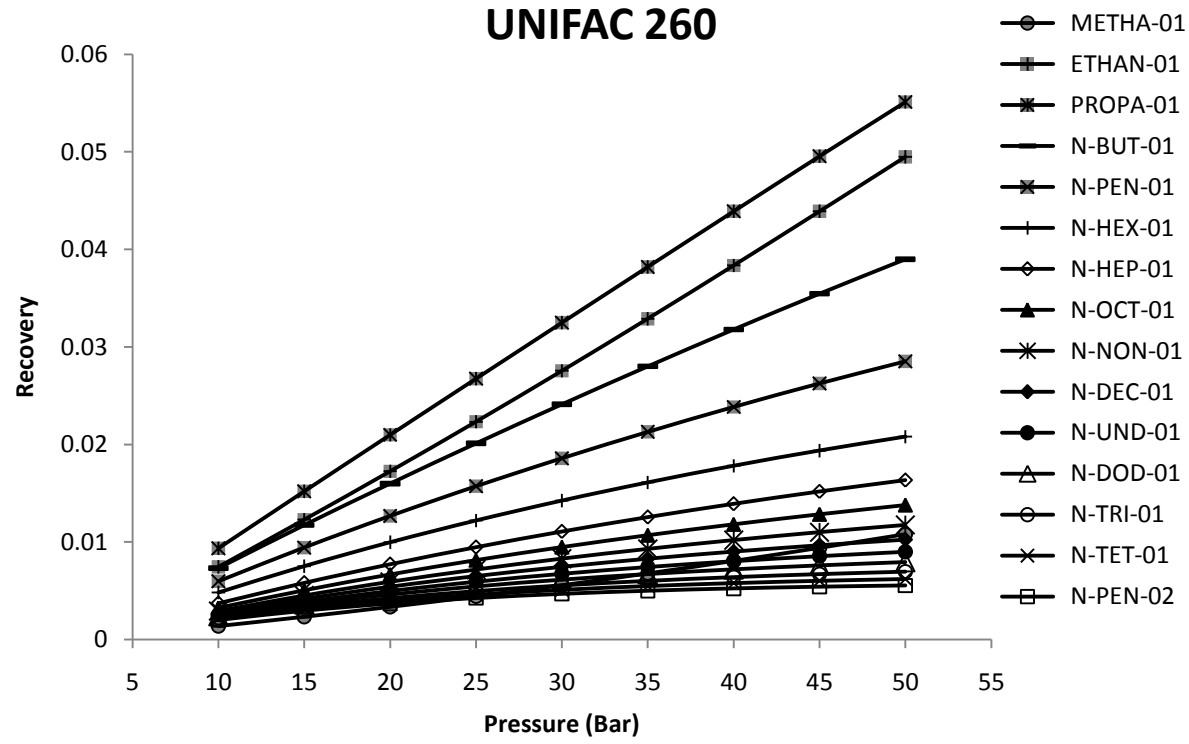

Figure B2. 11: UNIFAC model recovery results for hydrocarbons at 260˚C

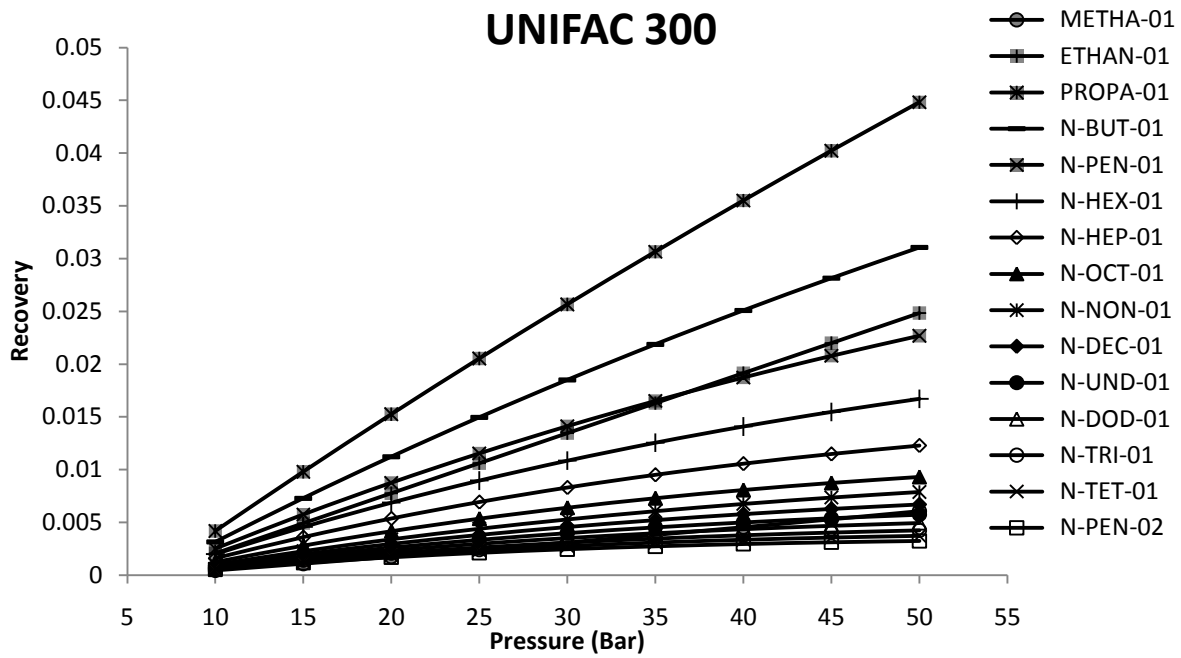

Figure B2. 12: UNIFAC model recovery results for hydrocarbons at 300˚C

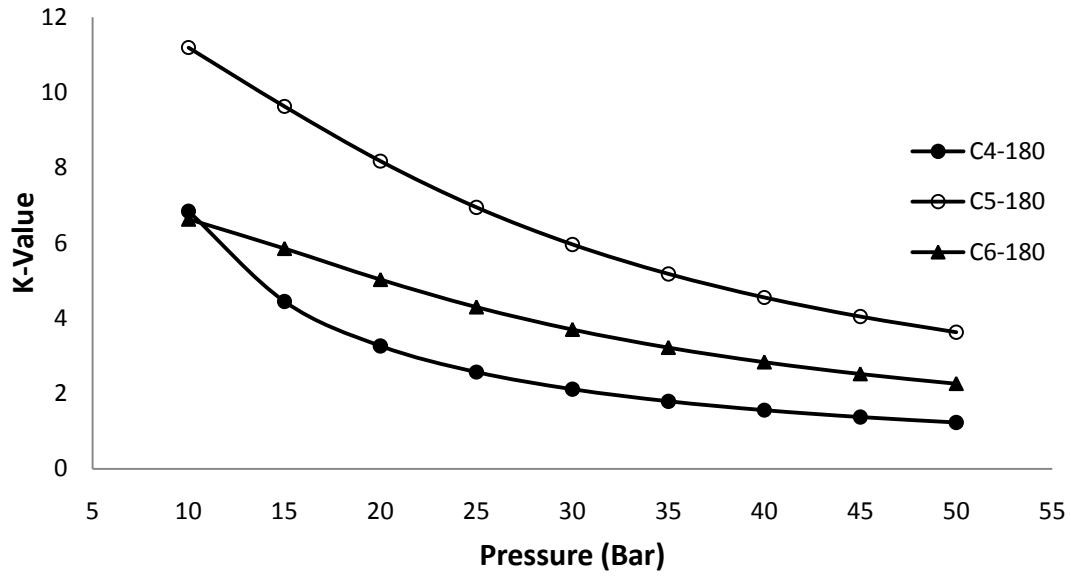

Figure B2. 13: K-values for C_4 to C_6 hydrocarbons at 180˚C

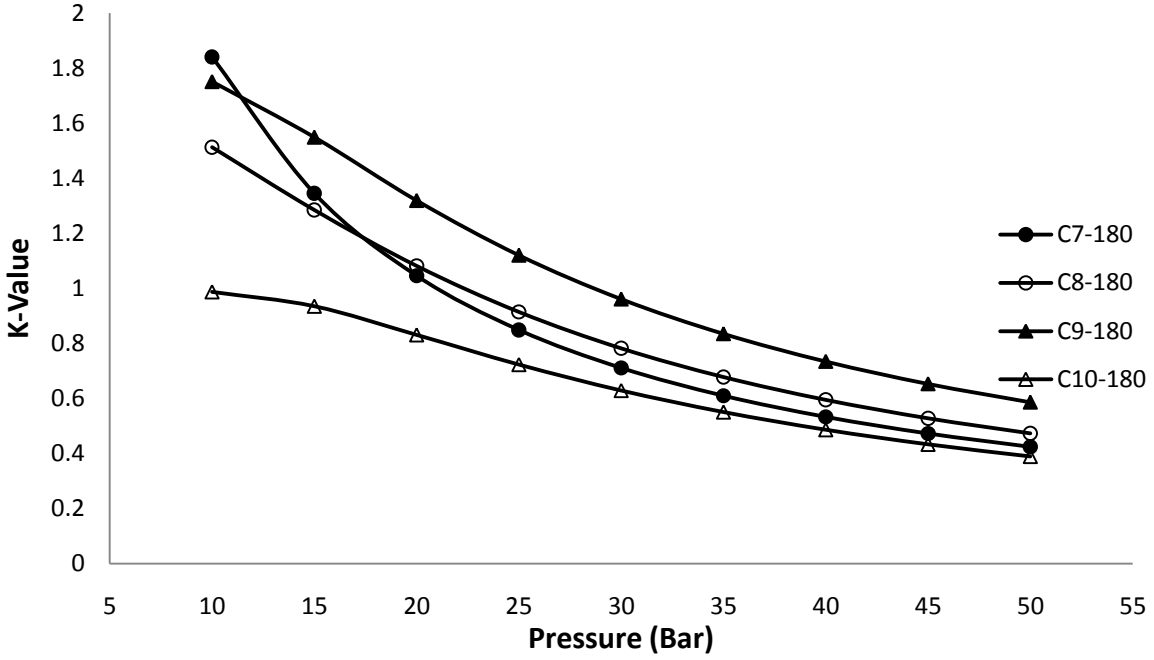

Figure B2. 14: K-values for C_7 to C_{10} hydrocarbons at 180˚C

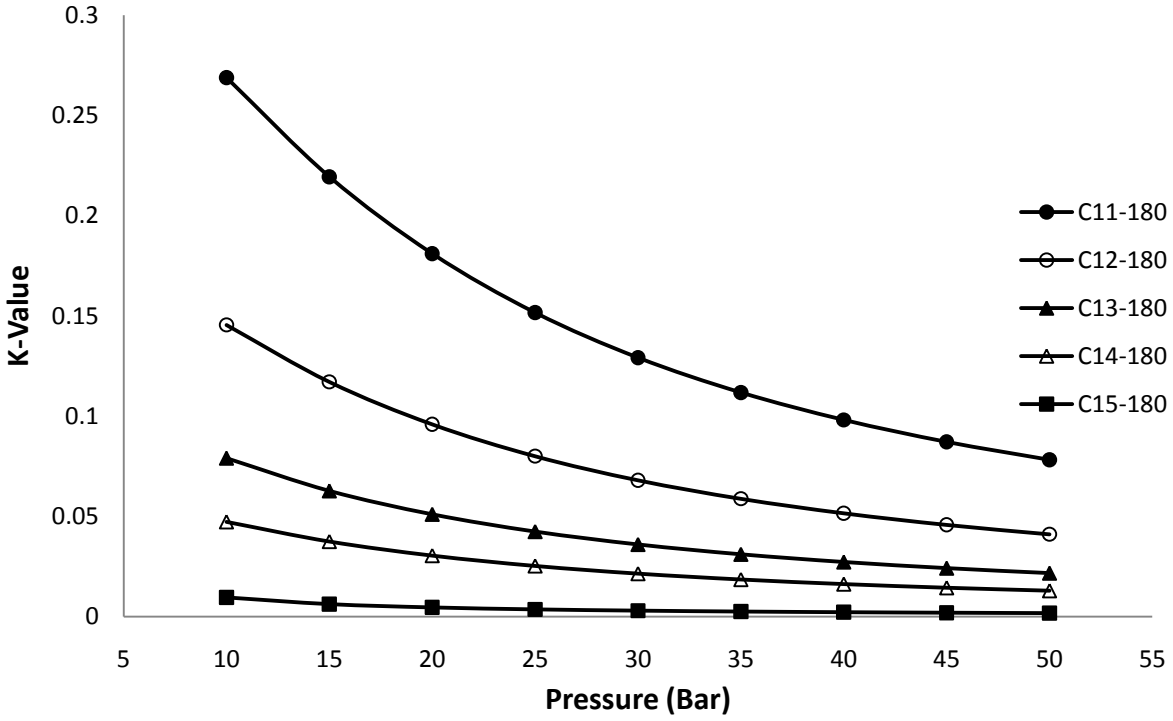

Figure B2. 15: K-values for C_{11} to C_{15} hydrocarbons at 180˚C

Appendix B3: Aspen Plus process simulation results

Table B3. 1: Aspen simulation results for glycerol water-removal process

	GLYCEROL	GLYMIXED	SYNGAS	FTPROD	LIQUID	FLIQUID	FVAPOUR	RECYCLE	FTWATER	TAILGAS
Substream: MIXED										
Mole flow kmol/s										
CARBO-01	0	8.31E-04	33.33333	6.933334	0.350785	8.31E-04	0.349954	8.31E-04	0.349954	6.58338
HYDRO-01	0	1.34E-09	66.66667	7.938066	6.00E-04	1.34E-09	6.00E-04	1.34E-09	6.00E-04	7.937466
WATER	0	3.408164	0	26.4	27.16558	3.40795	23.75763	3.408164	23.75763	2.642582
GLYCE-01	3.65	90.00146	0	0	89.8429	86.34835	3.494553	86.35146	3.494553	0.158558
METHA-01	0	1.63E-04	0	1.228961	0.061927	1.63E-04	0.061764	1.63E-04	0.061764	1.167197
ETHAN-01	0	4.69E-03	0	0.983169	0.281117	4.69E-03	0.276426	4.69E-03	0.276426	0.706741
PROPA-01	0	2.89E-03	0	0.786535	0.215253	2.89E-03	0.21236	2.89E-03	0.21236	0.574172
N-BUT-01	0	1.51E-03	0	0.629228	0.134235	1.51E-03	0.132721	1.51E-03	0.132721	0.496503
N-PEN-01	0	8.18E-04	0	0.503382	0.085345	8.18E-04	0.084527	8.18E-04	0.084527	0.418855
N-HEX-01	0	4.00E-04	0	0.402706	0.053165	4.00E-04	0.052765	4.00E-04	0.052765	0.349941
N-HEP-01	0	2.46E-04	0	0.322165	0.035389	2.46E-04	0.035143	2.46E-04	0.035143	0.287022
N-OCT-01	0	1.71E-04	0	0.257732	0.025422	1.71E-04	0.025251	1.71E-04	0.025251	0.232481
N-NON-01	0	1.23E-04	0	0.206185	0.018583	1.23E-04	0.01846	1.23E-04	0.01846	0.187726

N-DEC-01	0	9.21E-05	0	0.164948	0.013926	9.22E-05	0.013834	9.21E-05	0.013834	0.151114
N-UND-01	0	6.93E-05	0	0.131959	0.010462	6.93E-05	0.010393	6.93E-05	0.010393	0.121566
N-DOD-01	0	5.25E-05	0	0.105567	7.89E-03	5.25E-05	7.84E-03	5.25E-05	7.84E-03	0.097731
N-TRI-01	0	3.95E-05	0	0.084454	5.93E-03	3.96E-05	5.89E-03	3.95E-05	5.89E-03	0.078566
N-TET-01	0	3.04E-05	0	0.067563	4.51E-03	3.04E-05	4.48E-03	3.04E-05	4.48E-03	0.063083
N-PEN-02	0	2.34E-05	0	0.05405	3.43E-03	2.35E-05	3.41E-03	2.34E-05	3.41E-03	0.050641
Total Flow kmol/s	3.65	93.42177	100	47.2	118.3165	89.76846	28.54799	89.77177	28.54799	22.30532
Total Flow kg/s	336.1457	8350.645	1068.072	1068.072	8827.27	8014.209	813.0605	8014.499	813.0605	591.447
Total Flow m^3/s	0.2597781	7.402872	411.6331	73.89608	8.204762	7.14675	1165.184	7.147008	30.08917	36.72631
Temperature K	298.15	486.3172	493.15	493.15	516.756	493.15	493.15	493.15	298.15	500.1456
Pressure N/m^2	2.50E+06	2.50E+06	1.00E+06	2.50E+06	2.50E+06	1.00E+05	1.00E+05	2.50E+06	1.01E+05	2.50E+06
Enthalpy J/kmol	-6.68E+08	-6.12E+08	-3.11E+07	-1.60E+08	-5.31E+08	-6.10E+08	-2.68E+08	-6.10E+08	-3.25E+08	-8.56E+07
Enthalpy J/kg	-7.25E+06	-6.85E+06	-2.92E+06	-7.09E+06	-7.12E+06	-6.83E+06	-9.40E+06	-6.83E+06	-1.14E+07	-3.23E+06
Enthalpy Watt	-2.44E+09	-5.72E+10	-3.11E+09	-7.57E+09	-6.29E+10	-5.48E+10	-7.64E+09	-5.48E+10	-9.28E+09	-1.91E+09
Entropy J/kmol-K	-6.13E+05	-4.89E+05	30693.84	-55950.2	-3.95E+05	-4.84E+05	-71009	-4.84E+05	-2.18E+05	-59330.6
Entropy J/kg-K	-6651.966	-5466.05	2873.761	-2472.54	-5298.76	-5425.28	-2493.25	-5426.85	-7661.9	-2237.54
Density $kmol/m^3$	14.05045	12.61967	0.242935	0.638735	14.42046	12.56074	0.024501	12.56075	0.94878	0.607339
Density kg/m^3	1293.972	1128.028	2.594719	14.4537	1075.872	1121.378	0.697796	1121.378	27.0217	16.10418
Average MW	92.09472	89.3865	10.68072	22.62864	74.60729	89.27645	28.48048	89.27638	28.48048	26.51596
Liq Vol 60F m^3/s	0.2671899	6.65102	5.35578	1.925788	7.184732	6.383599	0.801132	6.38383	0.801132	1.392076

Table B3. 2: Sasol gas loop simulation results

	SYNGAS	FTPROD	COOLED	LIQUID	FLVAPOUR	COLDPLAN
Substream: MIXED						
Mole Flow kmol/s						
CARBO-01	33.33333	6.933334	6.933334	0.503177	6.430157	6.430157
HYDRO-01	66.66667	7.938066	7.938066	9.60E-07	7.938065	7.938065
WATER	0	26.4	26.4	26.36653	0.033465	0.033465
GLYCE-01	0	0	0	0	0	0
METHA-01	0	1.228961	1.228961	0.037759	1.191201	1.191201
ETHAN-01	0	0.983169	0.983169	0.016226	0.966943	0.966943
PROPA-01	0	0.786535	0.786535	0.010173	0.776362	0.776362
N-BUT-01	0	0.629228	0.629228	7.51E-03	0.621717	0.621717
N-PEN-01	0	0.503382	0.503382	5.66E-03	0.497724	0.497724
N-HEX-01	0	0.402706	0.402706	4.28E-03	0.398426	0.398426
N-HEP-01	0	0.322165	0.322165	3.32E-03	0.318848	0.318848
N-OCT-01	0	0.257732	0.257732	2.55E-03	0.255182	0.255182
N-NON-01	0	0.206185	0.206185	1.98E-03	0.204201	0.204201
N-DEC-01	0	0.164948	0.164948	1.56E-03	0.163393	0.163393
N-UND-01	0	0.131959	0.131959	1.25E-03	0.13071	0.13071
N-DOD-01	0	0.105567	0.105567	9.72E-04	0.104595	0.104595
N-TRI-01	0	0.084454	0.084454	7.65E-04	0.083688	0.083688
N-TET-01	0	0.067563	0.067563	5.88E-04	0.066974	0.066974
N-PEN-02	0	0.05405	0.05405	4.28E-04	0.053622	0.053622
Total Flow kmol/s	100	47.2	47.2	26.96473	20.23527	20.23527
Total Flow kg/s	1068.072	1068.072	1068.072	493.6595	574.4125	574.4125
Total Flow m^3/s	378.3068	73.89608	19.1629	0.505883	18.65702	33.0201
Temperature K	453.15	493.15	298.15	298.15	298.15	493.15
Pressure N/m^2	1.00E+06	2.50E+06	2.50E+06	2.50E+06	2.50E+06	2.50E+06
Enthalpy J/kmol	-3.23E+07	-1.60E+08	-1.94E+08	-2.82E+08	-7.58E+07	-6.36E+07
Enthalpy J/kg	-3.03E+06	-7.09E+06	-8.56E+06	-1.54E+07	-2.67E+06	-2.24E+06
Enthalpy Watt	-3.23E+09	-7.57E+09	-9.14E+09	-7.60E+09	-1.53E+09	-1.29E+09
Entropy J/kmol-K	28202	-55950.2	-1.36E+05	-1.59E+05	-1.04E+05	-73084

Entropy J/kg-K	2640.459	-2472.54	-5996.69	-8702.07	-3671.64	-2574.59
Density kmol/m^3	0.264336	0.638735	2.463093	53.30234	1.084593	0.612817
Density kg/m^3	2.823296	14.4537	55.73645	975.838	30.78801	17.39585
Average MW	10.68072	22.62864	22.62864	18.3076	28.38669	28.38669
Liq Vol 60F m^3/s	5.35578	1.925788	1.925788	0.511596	1.414192	1.414192